

Analytic trajectory bootstrap for matrix models

Wenliang Li

School of Physics, Sun Yat-Sen University, Guangzhou 510275, China

E-mail: liwliang3@mail.sysu.edu.cn

ABSTRACT: We revisit the large N two-matrix model with $\text{Tr}[A, B]^2$ interaction and quartic potentials by the analytic trajectory bootstrap, where A and B represent the two matrices. In the large N limit, we can focus on the single trace moments associated with the words composed of the letters A and B . Analytic continuations in the lengths of the words and subwords lead to analytic trajectories of single trace moments and intriguing intersections of different trajectories. Inspired by the one-cut solutions of one-matrix models, we propose some simple ansatzes for the singularity structure of the two-matrix generating functions and the corresponding single trace moments. Together with the self-consistent constraints from the loop equations, we determine the free parameters in the ansatzes and obtain highly accurate solutions for the two-matrix model at a low computational cost. For a given length cutoff L_{\max} , our results are within and more accurate than the positivity bounds from the relaxation method, such as about 6-digit accuracy for $L_{\max} = 18$. The convergence pattern suggests that we achieve about 8-digit accuracy for $L_{\max} = 22$. As the singularity structure is closely related to the eigenvalue distributions, we further present the results for various types of eigenvalue densities. In the end, we study the symmetry breaking solutions using more complicated ansatzes.

Contents

1	Introduction	1
2	One-matrix model	4
2.1	Resolvent and one-cut solutions	4
2.2	One-length trajectory bootstrap	5
3	Two-matrix model	6
3.1	Generating functions and one-cut solutions	7
3.2	One-length trajectory bootstrap	10
3.3	Two-length trajectory bootstrap	13
3.3.1	$L_{\max} = 6$	13
3.3.2	$L_{\max} = 10$	14
3.3.3	$L_{\max} = 14, 18, 22$	15
3.4	Eigenvalue distributions	18
4	Symmetry breaking solutions	21
4.1	One-matrix model	21
4.2	Two-matrix model	25
5	Discussion	29
A	Analytic ansatz from matrix integrals	31

1 Introduction

Regge trajectories first appeared in the phenomenological description of hadron physics, but later led to string theory as a promising candidate for the quantum theory of gravity. Intriguingly, Regge trajectories connect particles of the same properties except for the angular momentum and mass. Can we also connect the physical observables associated with the same angular momentum by analytic continuation? As there is no spatial coordinate in matrix models, it is natural to consider this kind of analytic continuation. In this work, we study the matrix models based on analytic continuations in the numbers of matrices along the lines of [1–3, 5, 6].

Recently, Lin proposed a bootstrap approach for the large N matrix models using the loop equations¹ and positivity requirements [10]. This method is similar in spirit to the positivity-based bootstrap methods for conformal field theory [11] and lattice gauge theory

¹The loop equations are special cases of the Dyson-Schwinger equations [7–9] in the context of gauge theories and matrix models.

[12] (See also [13–16] and [17, 18]). This positive bootstrap approach can be extended to the large N matrix quantum mechanics, in which the role of the Dyson-Schwinger equations in the Lagrangian formalism is played by some equations of motion in the Hamiltonian formalism [19].² As the self-consistent constraints are quadratic equations due to the large N factorization, it is numerically challenging to solve the resulting non-linear optimization problem. In [46], Kazakov and Zheng introduced a relaxation procedure that treats the quadratic terms as independent variables and replaces the nonlinear equalities by linear inequalities. In this way, the positivity conditions can be formulated as semi-definite programming and solved more systematically. In [46], they also discussed the relation between the positivity requirements in the bootstrap formulation and the positivity of the eigenvalue density supported only on the real axis. Later, this relaxation procedure was used to revisit the positive bootstrap for large N lattice Yang-Mills theory [47].³

In this work, we are mainly interested in the two-matrix model with $[A, B]^2$ interaction and quartic potential considered previously in [46], which is not analytically solvable by the known methods.⁴ We want to bootstrap this two-matrix model using the analytic trajectory approach, without relying on positivity requirements. Therefore, our approach is sharply different from many recent positive bootstrap studies mentioned above. We will present highly accurate results based on some ansatzes for the singularity structure of the generating functions. The challenges associated with the nonlinearity of the loop equations are partly tamed by these analytic ansatzes. As we make use of the fully nonlinear loop equations without using the relaxation procedure, we are able to surpass the accuracy of the positive bootstrap results in [46]. Nevertheless, we should stress that our study is crucially guided by the high-precision positivity bounds from the relaxation bootstrap in [46].

The basic idea of the analytic trajectory bootstrap for matrix models is associated with the large length limit. This is analogous to the large spin limit in the lightcone bootstrap for conformal field theory [51, 52], where the large spin asymptotic behavior is related to the lightcone singularity. For matrix models, the large length limit of the matrix moments is also similar to the thermodynamic limit. In statistical mechanics, we can write the partition function of a translation invariant lattice model as

$$Z = \text{tr } T^n = \sum_{\lambda \in S} \lambda^n \rho(\lambda) \xrightarrow{n \rightarrow \infty} \lambda_*^n \rho(\lambda_*), \quad (1.1)$$

where T is the transfer matrix that relates a sequence of subsystems, n is the number of subsystems, S is the support of the eigenvalue distribution, and ρ encodes the multiplicity of the discretely distributed eigenvalues. In the thermodynamic limit $n \rightarrow \infty$, there is an infinite number of subsystems and the free energy per site $F = \frac{1}{V} \log Z$ is dominated by

²See also the bootstrap studies of quantum mechanics [1, 5, 20–41] and quantum many body systems [42–45].

³See also the recent works [48, 49] on the positive bootstrap for finite N lattice Yang-Mills theory and abelian lattice gauge theories. As the loop equations are linear, there is no need to use the relaxation procedure in these studies.

⁴See [50] for a review of analytically solvable matrix models.

the contribution associated with the largest eigenvalue λ_* .⁵ As a landmark in theoretical physics, Onsager used the transfer matrix method [53, 54] to compute the exact free energy of the two-dimensional Ising model on a square lattice [55]. It was shown that the singular critical point can emerge in the analytic framework of statistical mechanics by taking the thermodynamic limit. One can also apply the transfer matrix method to the computation of correlation functions. For instance, the two-point function of the two-dimensional Ising model can be written as

$$\begin{aligned} \langle S_{i_1, j_1} S_{i_2, j_2} \rangle &= \frac{1}{Z} \text{tr}(\sigma_{i_1}^z T^{j_2 - j_1} \sigma_{i_2}^z T^{n - j_2 + j_1}) \\ &= \frac{1}{Z} \left\langle \hat{S}_{i_1, j_1} \hat{S}_{i_2, j_2} T^n \right\rangle \xrightarrow{n \rightarrow \infty} \left\langle 0 \left| \hat{S}_{i_1, j_1} \hat{S}_{i_2, j_2} \right| 0 \right\rangle, \end{aligned} \quad (1.2)$$

where $j_2 > j_1$ has been assumed, $S_{i, j}$ denotes the classical spin variable, and σ_i^z is the diagonal Pauli matrix associated with the i -th site. In the thermodynamic limit, the leading behavior of the two-point function can be interpreted as the vacuum expectation value of spin operators $\hat{S}_{i_1, j_1} \hat{S}_{i_2, j_2}$ in the Heisenberg picture, where the ground state is the eigenvector associated with the largest eigenvalue of the transfer matrix.

For matrix models, it is interesting to consider the large length limit due to a similar mechanism of maximum eigenvalue dominance.⁶ Although the basic idea is essentially the same, some minor modifications are needed because the density vanishes at the largest eigenvalues, which is different from the case of the transfer matrix. For two-matrix models, the Green's functions of identical and mixed matrices are analogous to the partition function (1.1) and correlation function (1.2). In the large length limit, the leading behavior of a long Green's function is closely related to the eigenvalues with the largest absolute values. The leading singularities of the generating functions should exhibit a simple structure. As the analogue of finite size corrections, the subleading terms in the large length limit should also take a relatively simple form. We expect that the minimally singular solutions of the two-matrix generating functions share some similarities with the one-cut solutions of the resolvents in the one-matrix models.

The large length expansion of the Green's functions gives rise to asymptotic series that do not converge as the truncation parameter increases. To resolve this issue, we propose some analytic ansatzes for the singularity structure, which in some sense resum the large length expansion. They are based on some conjectured form of the singularity structure of the generating functions. It turns out that they lead to rapidly convergent results even at $n = 0$, where n denotes the length of a full word or a subword. In this way, we are able to derive highly accurate solutions of the two-matrix model. Furthermore, we use a local minimization method to significantly reduce the computational cost.

In Sec. 2, we revisit one-cut solutions of the quartic one-matrix model from the analytic trajectory bootstrap perspective. In Sec. 3, we use the analytic trajectory bootstrap to derive highly accurate solutions of the two-matrix model, which can be viewed as a natural

⁵We assume that the multiplicity or density of eigenvalues remains finite at λ_* and all the eigenvalues are positive real. More generally, λ_* denotes the eigenvalues with the largest absolute values.

⁶In the large n limit, the significant role of the largest eigenvalues in the matrix models is similar to that of the eigen-energies in quantum mechanics [5, 6].

generalization of the one-cut solutions of one-matrix models. In Sec. 4, we extend this approach to the symmetry breaking solutions by introducing more complicated ansatzes. In Sec. 5, we summarize our results and discuss some directions for the future investigations. In Appendix A, we deduce the analytic ansatz for one-length Green's functions from the matrix integral perspective.

2 One-matrix model

2.1 Resolvent and one-cut solutions

In the large N one-matrix model ⁷

$$Z = \lim_{N \rightarrow \infty} \int dM e^{-N \text{tr} V(M)}, \quad (2.1)$$

the basic observables are the single trace moments of the Hermitian matrix M :

$$G_n = \langle \text{Tr} M^n \rangle, \quad (2.2)$$

where $\text{Tr} = \frac{1}{N} \text{tr}$ is the normalized trace. For the identity matrix, we have $\text{Tr} I = 1$. Following the standard procedure, we introduce the resolvent

$$R(z) = \left\langle \text{Tr} \frac{1}{z - M} \right\rangle = \sum_{n=0}^{\infty} G_n z^{-n-1}. \quad (2.3)$$

The matrix moments can be derived from a contour integral

$$G_n = \frac{1}{2\pi i} \oint_C dz z^n R(z) = \int_S dz z^n \rho(z), \quad (2.4)$$

where the contour C encircles anti-clockwise all the branch points of $R(z)$. The support S of the eigenvalue distribution and the eigenvalue density $\rho(x)$ are determined by the discontinuity of the resolvent $R(z)$. Usually, n is assumed to be a non-negative integer, but it is possible to consider a complex power n . In this way, G_n admits analytic continuation to complex n . See [6] for a closely related discussion for the complex-power expectation values in the context of quantum mechanics.

For a polynomial potential $V(x)$ with \mathbb{Z}_2 symmetry, the symmetric one-cut solutions in Brézin-Itzykson-Parisi-Zuber's classical work [57] can be written as ⁸

$$R(z) = \sum_{k=0}^{k_{\max}} a_k (z^2 - z_*^2)^{\frac{1}{2}+k} + \text{regular}, \quad (2.5)$$

where k_{\max} depends on the degree of $V(x)$. The branch points are located at $z = \pm z_*$ due to the \mathbb{Z}_2 symmetry. The series expansion of a building block for the one-cut resolvent

⁷See [56] for a review of various approaches to the matrix models.

⁸For symmetry breaking solutions, the building blocks for the one-cut solutions are $z^k \sqrt{(z - z_1)(z - z_2)}$, where $z_1 \neq -z_2$. See Sec. 4.1 for more details.

reads

$$\begin{aligned}
(z^2 - z_*^2)^{\frac{1}{2}+k} &= \sum_{j=0}^{\infty} \frac{(-1/2 - k)_j}{j!} z_*^{2j} z^{-2j+2k+1} \\
&= \frac{(-1/2 - k)_{k+1}}{(k+1)!} z_*^{2(k+1)} \sum_{\frac{n}{2}=-k-1}^{\infty} \frac{(1/2)_{n/2}}{(k+2)_{n/2}} z_*^n z^{-n-1}.
\end{aligned} \tag{2.6}$$

In order to match with the large z expansion of the resolvent $R(z)$ in (2.3), we have changed the summation variable from j to $n = 2(j - k - 1)$. The absence of odd n terms is related to the \mathbb{Z}_2 symmetry constraint $\langle \text{Tr} M^n \rangle = 0$ for odd n . Therefore, we obtain an analytic ansatz for the single trace moments

$$G_n = \frac{1 + (-1)^n}{2} \sum_{k=0}^{k_{\max}} b_k \frac{(1/2)_{n/2}}{(k+2)_{n/2}} z_*^n, \tag{2.7}$$

where $b_k = a_k \frac{(-1/2-k)_{k+1}}{(k+1)!} z_*^{2(k+1)}$. The k summation in (2.7) can be interpreted as a convergent expansion in large length n . The coefficients b_k will be determined by the large N Dyson-Schwinger equations

$$\langle \text{Tr} M^n V'(M) \rangle = \sum_{p=0}^{n-1} \langle \text{Tr} M^p \rangle \langle \text{Tr} M^{n-p-1} \rangle, \tag{2.8}$$

which are called the large N loop equations in the context of matrix models. We have omitted the subleading terms in the large N limit. The quadratic terms on the right hand side of (2.8) come from the large N factorization of the double trace moments. The summation over the different ways of cutting the word M^n can be encoded in the product of two resolvents, i.e., $R(z)^2$. As a result, $R(z)$ satisfies a quadratic equation and the branch points of $R(z)$ are of the square root type.

2.2 One-length trajectory bootstrap

Let us consider the concrete example of the quartic potential

$$V(M) = \frac{1}{2} M^2 + \frac{g}{4} M^4. \tag{2.9}$$

The loop equations read

$$G_{n+1} + g G_{n+3} = \sum_{p=0}^{n-1} G_p G_{n-p-1}. \tag{2.10}$$

There are two free parameters. If we set $G_0 = 1$, the other Green's functions can be expressed in terms of G_2 :

$$G_4 = \frac{1 - G_2}{g}, \quad G_6 = \frac{(2g + 1)G_2 - 1}{g^2}, \quad G_8 = \frac{g^2 G_2^2 - (4g + 1)G_2 + 2g + 1}{g^3}, \tag{2.11}$$

$$G_{10} = \frac{-3g^2 G_2^2 + (6g^2 + 6g + 1)G_2 - 4g - 1}{g^4}. \quad (2.12)$$

For symmetric one-cut solutions, it turns out that $k_{\max} = 1$ is sufficient for the analytic ansatz (2.7):

$$G_n = \frac{1 + (-1)^n}{2} \left(b_0 \frac{(1/2)_{n/2}}{(2)_{n/2}} + b_1 \frac{(1/2)_{n/2}}{(3)_{n/2}} \right) z_*^n, \quad (2.13)$$

which can be expressed as an integral (2.4) over the support of the eigenvalue distribution. The density of eigenvalues is given by

$$\rho(z) = \frac{1}{\pi z_*} \left(2b_0 \left(1 - \frac{z^2}{z_*^2} \right)^{1/2} + \frac{8}{3} b_1 \left(1 - \frac{z^2}{z_*^2} \right)^{3/2} \right). \quad (2.14)$$

Using the three relations for (G_4, G_6, G_8) in (2.11), we can fix the coefficients and G_2 :

$$b_0 = -1 + \frac{12}{z_*^2} - \frac{4(9g+1)}{4+3gz_*^2}, \quad b_1 = 1 - b_0, \quad G_2 = \frac{16 + gz_*^4}{4(4+3gz_*^2)}, \quad (2.15)$$

which are determined by the locations of the branch points $\pm z_*$. Although there remain infinitely many relations for $n > 8$, they are not independent and imply a polynomial equation for z_*^2 :

$$3g(z_*^2)^2 + 4z_*^2 - 16 = 0. \quad (2.16)$$

The two solutions of this quadratic equation read

$$z_{*,\pm}^2 = \frac{2}{3g} \left(-1 \pm \sqrt{12g+1} \right), \quad (2.17)$$

which give precisely the one-cut solutions for G_2

$$G_2^{(\text{one-cut}),\pm} = \frac{\pm(12g+1)^{3/2} - 18g - 1}{54g^2}. \quad (2.18)$$

For $g > 0$, the support of the eigenvalue distribution is on the real axis for the positive solution and on the imaginary axis for the negative solution. For $0 > g > -\frac{1}{12}$, both solutions are supported on the real axis. As g decreases, the two solutions meet at the critical point $g = -\frac{1}{12}$ and become a complex conjugate pair for $g < -\frac{1}{12}$.

3 Two-matrix model

The multi-matrix models are usually not analytic solvable by the known analytic methods. As a concrete example, we will consider the large N two-matrix model

$$Z = \lim_{N \rightarrow \infty} \int dA dB e^{-N \text{tr} V(A,B)}. \quad (3.1)$$

where the two-matrix potential reads

$$V(A, B) = \frac{1}{2} A^2 + \frac{g}{4} A^4 + \frac{1}{2} B^2 + \frac{g}{4} B^4 - \frac{h}{2} [A, B]^2. \quad (3.2)$$

Previously, this two-matrix model has been studied using the relaxation bootstrap [46] and the Monte Carlo method [58]. To make high precision comparison, we will focus on the Z_2 symmetric solutions for $g = h = 1$, as 6-digits results have been obtained in [46].

3.1 Generating functions and one-cut solutions

In the large N two-matrix model (3.2), the basic observables are the single trace moments of identical matrices

$$G_{n,0}^{(2)} = \langle \text{Tr} A^n \rangle, \quad G_{0,n}^{(2)} = \langle \text{Tr} B^n \rangle, \quad (3.3)$$

and the single trace moments of mixed matrices

$$G_{n_1, n_2, \dots, n_{2k-1}, n_{2k}}^{(2k)} = \langle \text{Tr} A^{n_1} B^{n_2} \dots A^{n_{2k-1}} B^{n_{2k}} \rangle, \quad (3.4)$$

where the superscript $(2k)$ indicates the number of length variables. For the mixed moments, we can take a contraction limit. For $k > 1$, we have

$$\lim_{n_j \rightarrow 0} G_{\dots, n_{j-1}, n_j, n_{j+1}, \dots}^{(2k)} = G_{\dots, n_{j-1} + n_{j+1}, \dots}^{(2k-2)}. \quad (3.5)$$

For $k = 1$, the mixed matrix moments reduce to identical matrix moments in (3.3)

$$\lim_{n_2 \rightarrow 0} G_{n_1, n_2}^{(2)} = \langle \text{Tr} A^{n_1} \rangle, \quad \lim_{n_1 \rightarrow 0} G_{n_1, n_2}^{(2)} = \langle \text{Tr} B^{n_2} \rangle. \quad (3.6)$$

As a natural generalization of the resolvents for identical matrix moments

$$R_A(z) = \left\langle \text{Tr} \left(\frac{1}{z - A} \right) \right\rangle, \quad R_B(z) = \left\langle \text{Tr} \left(\frac{1}{z - B} \right) \right\rangle, \quad (3.7)$$

we introduce the generating functions for the mixed moments (see e.g. [59])

$$\begin{aligned} R^{(2k)}(z_1, \dots, z_{2k}) &= \left\langle \text{Tr} \left(\frac{1}{z_1 - A} \frac{1}{z_2 - B} \dots \frac{1}{z_{2k-1} - A} \frac{1}{z_{2k} - B} \right) \right\rangle \\ &= \sum_{n_1=0}^{\infty} \dots \sum_{n_{2k}=0}^{\infty} z_1^{-n_1-1} \dots z_{2k}^{-n_{2k}-1} G_{n_1, \dots, n_{2k}}^{(2k)}. \end{aligned} \quad (3.8)$$

By construction, the generating functions obey some general constraints:

$$R^{(2k)}(z_1, z_2, z_3, z_4, \dots, z_{2k-1}, z_{2k}) = R^{(2k)}(z_3, z_4, \dots, z_{2k-1}, z_{2k}, z_1, z_2), \quad (3.9)$$

$$R^{(2k)}(z_1, z_2, z_3, \dots, z_{2k-1}, z_{2k}) = R^{(2k)}(z_1, z_{2k}, z_{2k-1}, \dots, z_3, z_2). \quad (3.10)$$

If the solution is symmetric under the \mathbb{Z}_2 transformation $A \leftrightarrow B$, we further have

$$R^{(2k)}(z_1, z_2, z_3, \dots, z_{2k}) = R^{(2k)}(z_2, z_3, \dots, z_{2k}, z_1). \quad (3.11)$$

We can recover the mixed moments by evaluating the contour integral

$$G_{n_1, \dots, n_{2k}}^{(2k)} = \left[\prod_{j=1}^{2k} \left(\frac{1}{2\pi i} \oint_C dz z^n \right)_j \right] R^{(2k)}(z_1, \dots, z_{2k}), \quad (3.12)$$

where the subscripts of (z_j, C_j) are indicated by $(\dots)_j$. Since the singularity structure of $R^{(2k)}$ is related to the support of the matrix eigenvalue distribution, we assume that there

are only branch point singularities, which are connected by branch cuts. The locations of the branch points in the z_j complex plane are determined by the corresponding large N matrix. The contour C_j encircles all the branch points in the z_j complex plane.

For $A \leftrightarrow B$ symmetric solutions, the locations of the branch points are expected to be the same in all the $\{z_j\}$ complex planes. However, the discontinuity of $R^{(2k)}$ on the support is not necessarily a factorized function in (z_1, \dots, z_{2k}) due to the relative ‘‘angle’’ between A and B . As in the one-matrix model, we focus on the $\mathbb{Z}_2 \times \mathbb{Z}_2 \times \mathbb{Z}_2$ symmetric one-cut solutions

$$R^{(2k)}(z_1, \dots, z_{2k}) = \sum_{k_1=0}^{\infty} \cdots \sum_{k_{2k}=0}^{\infty} a_{k_1, \dots, k_{2k}}^{(2k)} \prod_{j=1}^{2k} (z_j^2 - z_*^2)^{\frac{1}{2} + k_j} + \text{regular}, \quad (3.13)$$

where the coefficients $a_{k_1, \dots, k_{2k}}$ should be compatible with (3.9), (3.10), (3.11). To minimize the complexity of the singularity structure [5], we assume that the branch point singularities are essentially of the square-root type, i.e., they involve half-integer powers.

By construction, the generating function $R^{(2k)}(z_1, \dots, z_{2k})$ should be regular at infinity. In (3.13), we assume that the branch point singularities at finite $\{z_j\}$ are encoded in the $\{k_j\}$ summations. We will further assume that the $\{k_j\}$ summations are convergent, i.e., their finite truncations give more and more accurate approximations for the singularity structure as the truncation cutoff increases. The ‘‘singularity’’ expansion and the large length expansion are similar in spirit to the lightcone bootstrap and the large spin expansion in the context of conformal field theory [51, 52, 60–64]. For the matrix models, we can partly resum the large length expansion due to the simpler singularity structure. As we will see, the k summation is rapidly convergent even at small length.

There are infinitely many generating functions and their complexity grows with the number of $\{z_j\}$ variables. In practice, we consider a finite subset of generating functions. In this work, we study two simple scenarios:

1. In the first scenario, we consider only one-length observables as in the case of one-matrix models. The single-trace moments take the form

$$\langle \text{Tr } A^n \mathcal{O} \rangle. \quad (3.14)$$

Some simple examples are $\mathcal{O} = I, B^2, ABAB, BA^2B, B^4$. To study the analytic behavior in n , we introduce the generalized resolvent

$$R_{\mathcal{O}}(z) = \left\langle \text{Tr} \frac{\mathcal{O}}{z - A} \right\rangle = \sum_{n=0}^{\infty} \langle \text{Tr } \mathcal{O} A^n \rangle z^{-n-1}, \quad (3.15)$$

which are related to the generating function $R^{(2k)}(z_1, \dots, z_{2k})$ by certain contour integrals. The standard resolvent corresponds to the case of the identity operator I . As in (3.13), we assume that the one-cut solution of a generalized resolvent involves an infinite sum of $(z^2 - z_*^2)^{\frac{1}{2} + k}$ with $k = 0, 1, 2, \dots$. After truncating the k summation, a generalized resolvent is approximated by

$$R_{\mathcal{O}}(z) \approx \sum_{k=0}^{k_{\max}} a_{k, \mathcal{O}} (z^2 - z_*^2)^{\frac{1}{2} + k} + \text{regular}. \quad (3.16)$$

Therefore, the analytic ansatz for the one-length Green's functions are given by

$$\langle \text{Tr } \mathcal{O} A^n \rangle \approx \sum_{k=0}^{k_{\max}} b_{k, \mathcal{O}} \frac{(1/2)_{n/2}}{(k+2)_{n/2}} z_*^n, \quad (3.17)$$

According to the $A \rightarrow -A$ symmetry, there exists an implicit factor, depending on the number of A in \mathcal{O} . If \mathcal{O} contains an even number of A , the factor is $\frac{1+(-1)^n}{2}$.

2. In the second scenario, we focus on the simplest multi-length observables

$$G_{n_1, n_2}^{(2)} = \langle \text{Tr } A^{n_1} B^{n_2} \rangle, \quad (3.18)$$

which contain two length variables. They reduce to the identical matrix moments in a contraction limit $n_j \rightarrow 0$. In the approximate one-cut solutions, the k_j summations in the two-length generating function are truncated to finite sums:

$$R^{(2)}(z_1, z_2) \approx \sum_{k_1=0}^{k_{\max}} \sum_{k_2=0}^{k_{\max}-k_1} a_{k_1, k_2}^{(2)} (z_1^2 - z_*^2)^{\frac{1}{2}+k_1} (z_2^2 - z_*^2)^{\frac{1}{2}+k_2} + \text{regular}. \quad (3.19)$$

Accordingly, the analytic ansatz for the two-length Green's functions reads

$$G_{n_1, n_2} \approx \sum_{k_1=0}^{k_{\max}} \sum_{k_2=0}^{k_{\max}-k_1} b_{k_1, k_2} \frac{(1/2)_{n_1/2} (1/2)_{n_2/2}}{(k_1+2)_{n_1/2} (k_2+2)_{n_2/2}} z_*^{n_1+n_2}, \quad (3.20)$$

where the $A \leftrightarrow B$ symmetry implies $b_{k_1, k_2} = b_{k_2, k_1}$. We do not write the superscript (2) and the factors $\frac{1+(-1)^{n_1}}{2} \frac{1+(-1)^{n_2}}{2}$ explicitly for notational simplicity. The additional factors are associated with the invariance under the transformations $A \rightarrow -A$ and $B \rightarrow -B$.

As in the one-matrix model examples, the free parameters will be determined by the large N loop equations

$$\langle \text{Tr } \mathcal{O} [A + gA^3 - h(2BAB - ABB - BBA)] \rangle = \sum_{p=1}^n \left\langle \text{Tr } \mathcal{O}_{p-1}^{(A, l)} \right\rangle \left\langle \text{Tr } \mathcal{O}_{n-p}^{(A, r)} \right\rangle, \quad (3.21)$$

where n denotes the length of the subword \mathcal{O} . The loop equations associated with the B derivative is redundant due to the $A \leftrightarrow B$ symmetry. As a two-matrix generalization of (2.8), the right hand side of (3.21) is summing over all possible ways of splitting \mathcal{O} according to the position of A , i.e., the p -th summand vanishes if the p -th letter of \mathcal{O} is B . We use the superscript l or r to indicate the left or right subword. See the Appendix E of [46] for some concrete examples of the loop equations for short words.

The loop equations in (3.21) imply that the Green's functions are related to each other. It turns out that only a small number of them are free parameters. All the Green's functions can be expressed in terms of the two-length Green's functions $G_{n_1, n_2} = \langle \text{Tr } A^{n_1} B^{n_2} \rangle$, where the one-length Green's functions $G_n = \langle \text{Tr } A^n \rangle = \langle \text{Tr } B^n \rangle$ are the special cases with $n_1 = 0$

or $n_2 = 0$. We choose the expectation values of the one-length words and the simplest type of two-length words as the independent parameters:

$$G_{4j+2}, \quad G_{4j+4}, \quad G_{2,4j+2}, \quad (3.22)$$

where $j = 0, 1, 2, \dots$ ⁹ For notational simplicity, we will not write the superscript of the Green's functions explicitly. The normalized trace indicates $G_0 = 1$. Some explicit solutions associated with the short words are

$$G_{1,1,1,1} = \frac{1}{2}(-1 + G_2 + G_4 + 2G_{2,2}), \quad G_{2,4} = \frac{1}{6}(1 + G_2 - 6G_{2,2} + G_6), \quad (3.23)$$

$$G_{1,1,1,3} = \frac{1}{6}(1 - 5G_2 + 3G_4 - 6G_{2,2} + 4G_6), \quad G_{1,2,1,2} = -G_2 + G_4 - G_{2,2} + G_6, \quad (3.24)$$

$$G_{1,1,1,5} = \frac{1}{2}(-(G_2)^2 - 2G_4 + G_6 + G_8 + 2G_{2,6}), \quad (3.25)$$

$$G_{1,2,1,4} = \frac{1}{3}(1 - 8G_2 - 14(G_2)^2 - G_4 - 14G_{2,2} + 13G_6 + 6G_8 + 12G_{2,6}), \quad (3.26)$$

$$G_{4,4} = \frac{1}{6}(-3 + 15G_2 + 22(G_2)^2 - 4G_4 + 34G_{2,2} - 21G_6 - 6G_8 - 18G_{2,6}). \quad (3.27)$$

We notice that a Green's function of length- n can be expressed in terms of the independent ones in (3.22) of at most length- n . For $n \geq 8$, the solutions contain quadratic terms in the independent parameters. We also find higher order terms for larger length- n , such as cubic terms for $n = 14$ and quartic terms for $n = 20$.

In the first scenario, some intricate matching conditions for the one-length ansatz arise at the trajectory intersections due to the contraction limits and the symmetries of the Green's functions. Some of them can be automatically taken into account by the two-length ansatz in the second scenario. As we will see, the second scenario leads to a more systematic procedure and highly accurate solutions for the two-matrix model (3.2).

3.2 One-length trajectory bootstrap

The one-length trajectories exhibit intriguing intersection phenomena. The intersections can be associated with the contraction limit, such as

$$\langle \text{Tr } A^2 \rangle = \langle \text{Tr } A^2 B^0 \rangle, \quad \langle \text{Tr } BA^2 B \rangle = \langle \text{Tr } BA^2 BA^0 \rangle, \quad (3.28)$$

⁹If we set $g = h = 1$ before solving the loop equations, it may appear that there are additional independent parameters for long words. Since the solutions of the loop equations should be analytic in g and h around $g = h = 1$, we further impose that the loop equations are solved for $h = 1 + \delta h$ to first order in δh . In this way, we eliminate the additional independent parameters by the analyticity requirement. All Green's functions are determined by the independent ones in (3.22). For instance, we find one more free parameter at $L_{\max} = 12$ and fix it by solving the loop equations to first order in $\delta h = h - 1$.

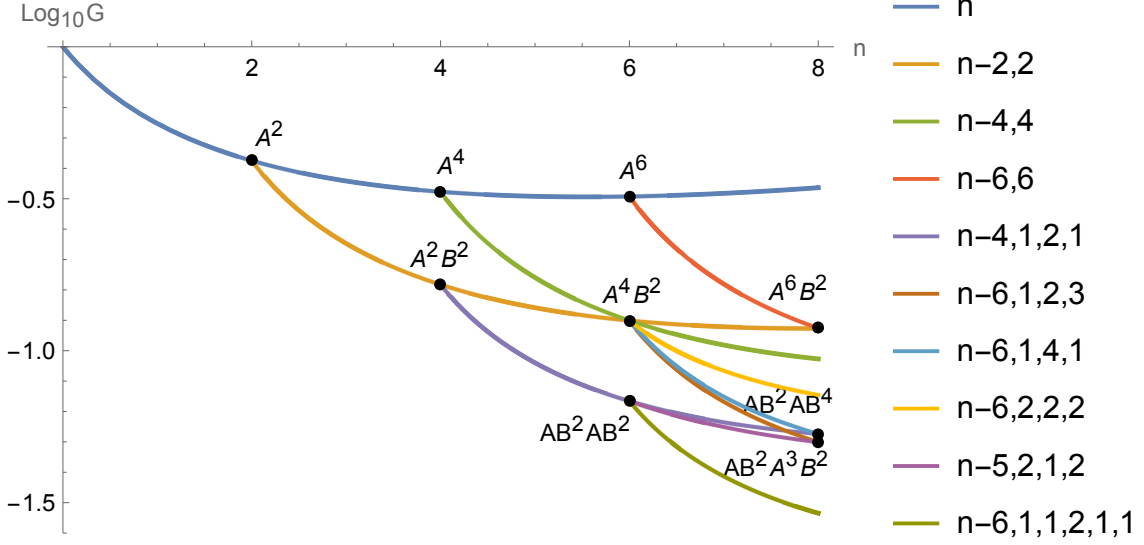


Figure 1: The analytic trajectories associated with the Green's functions $\langle \text{Tr} A^{n-L_{\mathcal{O}}} \mathcal{O} \rangle$ of the two-matrix model (3.2). Here n is the length of the full word $A^{n-L_{\mathcal{O}}} \mathcal{O}$, and $L_{\mathcal{O}}$ is the length of the subword \mathcal{O} . The trajectories are labelled by the powers of the letters as in (3.4). According to the contraction limit (3.5) and symmetries of the Green's functions, these analytic trajectories exhibit intriguing intersection phenomena, which lead to nontrivial matching conditions for the one-length analytic ansatz (3.17). We write down some explicit words associated the intersection points. For simplicity, we have stripped off the common factor $(1 + (-1)^n)/2$ associated with \mathbb{Z}_2 symmetry.

They can also be related to the symmetries of the Green's functions, such as

$$\langle \text{Tr} A^2 B^2 \rangle = \langle \text{Tr} B^2 A^2 \rangle = \langle \text{Tr} B A^2 B \rangle . \quad (3.29)$$

Assuming the invariance under the transformation $A \leftrightarrow B$, we can always use $\langle \text{Tr} A^n \mathcal{O} \rangle$ to represent a one-length trajectory. Some examples for the trajectory intersections are:

- Intersection at $n = 2$

$$\langle \text{Tr} A^n \rangle = \langle \text{Tr} A^{n-2} B^2 \rangle . \quad (3.30)$$

- Intersections at $n = 4$

$$\langle \text{Tr} A^n \rangle = \langle \text{Tr} A^{n-4} B^4 \rangle , \quad \langle \text{Tr} A^{n-2} B^2 \rangle |_{n=4} = \langle \text{Tr} A^{n-4} B A^2 B \rangle |_{n=4} . \quad (3.31)$$

- Intersections at $n = 6$

$$\langle \text{Tr} A^n \rangle = \langle \text{Tr} A^{n-6} B^6 \rangle , \quad (3.32)$$

$$\begin{aligned} \langle \text{Tr} A^{n-2} B^2 \rangle &= \langle \text{Tr} A^{n-4} B^4 \rangle = \langle \text{Tr} A^{n-6} B A^4 B \rangle \\ &= \langle \text{Tr} A^{n-6} B^2 A^2 B^2 \rangle = \langle \text{Tr} A^{n-6} B A^2 B^3 \rangle , \end{aligned} \quad (3.33)$$

$$\langle \text{Tr} A^{n-4} B A^2 B \rangle = \langle \text{Tr} A^{n-5} B^2 A B^2 \rangle = \langle \text{Tr} A^{n-6} B A B^2 A B \rangle . \quad (3.34)$$

Here we write the explicit Green's functions in terms of the letters A and B .

In Fig. 1, we present the one-length trajectories as analytic functions of the length of the complete word, which is based on the $L_{\max} = 12$ solutions. We can see more explicitly the intersection phenomena described above. We restrict to a subset of the trajectories that is connected to $G_{0,0} = \langle \text{Tr} I \rangle = 1$. The maximal word length is $n_{\max} = 8$. We use the more concise notation introduced in (3.4) to denote various one-length trajectories of the Green's functions.

L_{\max}	k_{\max}	z_*^2	$\langle \text{Tr} A^2 \rangle$	$\langle \text{Tr} A^4 \rangle$	$\langle \text{Tr} A^2 B^2 \rangle$
6	0	1.5769834	0.39424586	0.31085960	0.15542980
8	1	1.4940026	0.41986057	0.33095185	0.16422691
10	1	1.4942817	0.42341198	0.33496772	0.16508449
10	2	1.4939148	0.42308874	0.33464996	0.16506880
12	1	1.4930493	0.41616840	0.32669520	0.15533998
12	2	1.4960073	0.42178579	0.33333764	0.16495112

Table 1: The one-length trajectory bootstrap results of the two-matrix model (3.2) with $g = h = 1$, where we present 8 significant digits for the largest eigenvalue square and the independent Green's functions of length-2 and length-4. More accurate results from the two-length trajectory bootstrap are presented in Table 2.

In Table 1, we summarize the results of the one-length trajectory bootstrap for $L_{\max} \leq 12$. For a given length cutoff L_{\max} , we choose a truncation order k_{\max} for the analytic ansatzes in (3.17). Then we solve the matching conditions associated with the trajectory intersections and minimize the η function

$$\eta = (G_0 - 1)^2 + \left(G_{1,1,1,1} - \frac{1}{2}(-1 + G_2 + G_4 + 2G_{2,2}) \right)^2 + \left(G_{2,4} - \frac{1}{6}(1 + G_2 - 6G_{2,2} + G_6) \right)^2 + \dots , \quad (3.35)$$

which is constructed from the loop equations solutions with length not greater than L_{\max} and the Green's functions are replaced by (3.17). If k_{\max} is too small, we are not able to solve the matching conditions associated with the trajectory intersections. If k_{\max} is too large, the number of free parameters is greater than the number of constraints and the system is underdetermined, then we cannot solve for z_*^2 and the coefficients in the ansatzes for the one-length trajectories. Therefore, we find only one or two choices for k_{\max} for a given $L_{\max} \leq 12$. For the same L_{\max} , the accuracy increases with the truncation order k_{\max} of the analytic ansatzes.

As L_{\max} increases, there are more matching conditions from the intricate intersections of different trajectories. Furthermore, the number of coefficients in the analytic ansatzes also increases rapidly. As a result, the computational complexity grows rapidly. Below, we

will consider the two-length trajectory bootstrap, whose results can be improved in a more systematic way and at a lower computational cost.

3.3 Two-length trajectory bootstrap

Above, the matching conditions associated with the intersections of the one-length trajectories are imposed one by one. In fact, these constraints are encoded in the multi-length generating functions $R^{(2k)}(z_1, \dots, z_{2k})$. As different one-length trajectories are unified by the multi-length trajectories, analyticity guarantees that the results are independent of the path of analytic continuations. Below, we consider the simplest multi-length generating functions, i.e. $R^{(2)}(z_1, z_2)$ for the two-length Green's functions. At the price of one more variable, the matching conditions $\langle \text{Tr} A^{n_1} \rangle = \langle \text{Tr} A^{n_1} B^{n_2} \rangle|_{n_2 \rightarrow 0}$ can be satisfied automatically. According to the pattern of the independent parameters in (3.22), it is natural to set the length cutoff as $L_{\max} = 4p + 6$, where p is a non-negative integer. For a specific k_{\max} in the analytic ansatz (3.37), the number of free parameters in (3.20) is the same as that of constraints for the two-length Green's functions with the length cutoff $L_{\max} = 2k_{\max} + 6$, so we set $k_{\max} = 2p$.¹⁰ Below, we consider the cases of $p = 0, 1, 2, 3, 4$, so we set $L_{\max} = 6, 10, 14, 18, 22$.

3.3.1 $L_{\max} = 6$

For $L_{\max} = 6$, the constraints for the two-length Green's functions are

$$G_{0,0} = 1, \quad G_{2,4} = \frac{1}{6} (1 + G_2 - 6G_{2,2} + G_6), \quad (3.36)$$

where the first one is the normalization condition and the second one is derived from the loop equations. This corresponds to the lowest truncation order $k_{\max} = 0$, so the analytic ansatz for two-length Green's functions takes a factorized form

$$\langle \text{Tr} A^{n_1} B^{n_2} \rangle = b_{0,0} \frac{(1/2)_{n_1/2} (1/2)_{n_2/2}}{(2)_{n_1/2} (2)_{n_2/2}} z_*^{n_1} z_*^{n_2}, \quad (3.37)$$

where z_*^2 and $b_{0,0}$ are free parameters. The constraints (3.36) imply $b_{0,0} = 1$ and a degree-3 polynomial for z_*^2 :

$$7(z_*^2)^3 + 24(z_*^2)^2 - 16(z_*^2) - 64 = 0. \quad (3.38)$$

There are three solutions for z_*^2 . Only one solution is positive real and the other two solutions are negative real. In this work, we are mainly interested in the solution with eigenvalue support on the real axis, so we focus on the positive solution, which reads

$$z_*^2 \approx 1.59552. \quad (3.39)$$

Accordingly, the short Green's functions from the analytic ansatz (3.37) are

$$\langle \text{Tr} A^2 \rangle = \frac{z_*^2}{4} \approx 0.39888, \quad \langle \text{Tr} A^4 \rangle = \frac{z_*^4}{8} \approx 0.31821, \quad \langle \text{Tr} A^2 B^2 \rangle = \frac{z_*^4}{16} \approx 0.15911, \quad (3.40)$$

¹⁰In fact, we also examine the cases of $k_{\max} = 1, 3, 5, 7$. The results also converge to our highly accurate solution at $k_{\max} = 8$. However, their convergence rate is lower than the cases of even k_{\max} and obscures the rapid convergence pattern of even k_{\max} .

which are closely related to each other due to the simple form of the ansatz in (3.37). Our $L_{\max} = 6$ result for $\langle \text{Tr}A^2 \rangle$ in (3.40) is consistent with the positivity bounds for $L_{\max} = 8$ from the relaxation method in [46]:

$$0.393566 \leq \langle \text{Tr}A^2 \rangle \leq 0.431148. \quad (3.41)$$

3.3.2 $L_{\max} = 10$

To increase the truncation order for the analytic ansatz to $k_{\max} = 2$, we set the length cutoff as $L_{\max} = 10$. The free parameters in the analytic ansatz (3.20) are

$$z_*^2, \quad b_{0,0}, \quad b_{0,1}, \quad b_{0,2}, \quad b_{1,1}. \quad (3.42)$$

For $L_{\max} = 10$, the self-consistent constraints for the Green's functions are associated with

$$G_{0,0}, \quad G_{2,4}, \quad G_{4,4}, \quad G_{2,8}, \quad G_{4,6}. \quad (3.43)$$

We can see explicitly that the numbers of free parameters and constraints do match. The explicit constraints are (3.36), (3.27), and

$$G_{2,8} = \frac{1}{450} \left(-52 + 572G_2 + 84G_4 + 876G_{2,2} - 757G_6 - 378G_8 - 1206G_{2,6} - 45G_{10} + G_2(849G_2 + 426G_4 + 252G_{2,2}) \right), \quad (3.44)$$

$$G_{4,6} = \frac{1}{30} \left(11 - 61G_2 + 8G_4 - 128G_{2,2} + 86G_6 + 54G_8 + 48G_{2,6} + 15G_{10} - G_2(107G_2 + 18G_4 + 6G_{2,2}) \right). \quad (3.45)$$

They lead to nontrivial constraints for the independent Green's functions with $L_{\max} = 10$ in (3.22). In this case, we obtain a degree-25 polynomial for z_*^2 , and the coefficients $\{b_{k_1, k_2}\}$ are given by degree-24 polynomials in z_*^2 .¹¹ Among the 25 solutions, we find seven pairs of complex conjugate solutions and eleven real solutions, but only two of them are positive real:

$$z_*^2 \approx 1.49915, \quad 2.13966. \quad (3.46)$$

According to the $L_{\max} = 6$ result, the first solution seems more reliable. We will focus on the solution around $z_*^2 \approx 1.5$ below. Then we further determine the coefficients b_{k_1, k_2} and the Green's functions, such as

$$\langle \text{Tr}A^2 \rangle \approx 0.423552, \quad \langle \text{Tr}A^4 \rangle \approx 0.334978, \quad \langle \text{Tr}A^2 B^2 \rangle \approx 0.165201, \quad (3.47)$$

which should be more accurate than those in (3.40). As expected, our $L_{\max} = 10$ determination of $\langle \text{Tr}A^2 \rangle$ is also within the $L_{\max} = 8$ bounds in (3.41). Since the positivity bounds for $L_{\max} = 10, 12$ are not presented in [46], we are not able to make more comparisons with the positivity bounds from the relaxation bootstrap.

¹¹We use Mathematica's `GroebnerBasis` to derive the degree-25 polynomial equation in z_*^2 , and the expressions of b_{k_1, k_2} in terms of degree-24 polynomials in z_*^2 .

3.3.3 $L_{\max} = 14, 18, 22$

It is straightforward to apply the above procedure to higher truncation orders. We first need to solve the longer loop equations and express the two-length Green's functions in terms of the independent variables in (3.22). As the number of loop equations grow rapidly with L_{\max} , this step becomes computationally more and more expensive. After solving the loop equations, we use the relations between the two-length Green's functions to determine the free parameters in the analytic ansatz (3.20). We will use a local minimization method to extract the target solution of a set of polynomial equations, which is applicable to non-positive solutions and computationally cheaper than the positivity-based optimization methods. Our approach will not give rigorous bounds, so it is more difficult to estimate the errors in the results.

As the length cutoff L_{\max} increases, we need to solve a large system of high degree polynomial equations, so it becomes more and more challenging to obtain all the solutions. Using the trick in [6], we transform this difficult problem into a local minimization problem by introducing the η function

$$\begin{aligned} \eta = & (G_{0,0} - 1)^2 + \left(G_{2,4} - \frac{1 + G_2 - 6G_{2,2} + G_6}{6} \right)^2 \\ & + \left(G_{4,4} - \frac{1}{6}(-3 + 15G_2 + 22G_2^2 - 4G_4 + 34G_{2,2} - 21G_6 - 6G_8 - 18G_{2,6}) \right)^2 \\ & + \dots, \end{aligned} \tag{3.48}$$

which encodes the normalization condition and the self-consistent constraints for the two-length Green's functions from the loop equations, such as those in (3.36) and (3.27). In (3.48), we should substitute G_{n_1, n_2} with the analytic ansatz (3.20), so η is a function of the largest eigenvalue squared z_*^2 and the coefficients b_{k_1, k_2} of the building blocks in (3.20). The z_*^2 dependence is highly nonlinear. However, we find it easy to minimize the η function at a fixed z_*^2 despite the nonlinear dependence on b_{k_1, k_2} .

For $L_{\max} = 14$, the positive real solutions for z_*^2 of the polynomial system are $z_*^2 \approx 1.496, 1.694, 2.360, 5.205$. The first solution at $L_{\max} = 14$ can be identified with the first solutions in (3.39), (3.46) at lower truncation orders. Based on the one-length trajectory bootstrap results in Table 1 and the two-length trajectory bootstrap results for $L_{\max} = 6, 10, 14$, we conjecture that the exact solution is located around $z_*^2 \approx 1.5$. Accordingly, we find only one local minimum around $z_*^2 \approx 1.5$ at the higher length cutoff $L_{\max} = 18, 22$ and obtain rapidly convergent results. As we are mainly interested in the solutions with $z_*^2 \approx 1.5$, the starting values for the local minimization should be chosen properly. In practice, we first determine the starting values of b_{k_1, k_2} by minimizing the $\eta|_{z_*^2=1.5}$ function where z_*^2 is near the conjectured exact value. Then we carry out a local minimization with 1.5 as the starting value for z_*^2 . In spite of high nonlinearity, we always obtain a local minimum with an extremely small η_{\min} , which approaches zero as the working precision increases. Then we substitute the η minimization results into the analytic ansatz (3.20). This allows us to evaluate the two-length Green's functions and thus all single-trace moments of the target solution.

L_{\max}	k_{\max}	z_*	$\langle \text{Tr}A^2 \rangle$	$\langle \text{Tr}A^4 \rangle$	$\langle \text{Tr}A^2B^2 \rangle$
6	0	<u>1.263139202</u>	<u>0.3988801608</u>	<u>0.3182107654</u>	<u>0.1591053827</u>
10	2	<u>1.224398880</u>	<u>0.4235522795</u>	<u>0.3349775096</u>	<u>0.1652013401</u>
14	4	<u>1.223020278</u>	<u>0.4217471346</u>	<u>0.3333103568</u>	<u>0.1649495485</u>
18	6	<u>1.223040962</u>	<u>0.4217835573</u>	<u>0.3333413331</u>	<u>0.1649530130</u>
22	8	<u>1.223041990</u>	<u>0.4217840726</u>	<u>0.3333417063</u>	<u>0.1649530476</u>

Table 2: The two-length trajectory bootstrap results for the largest eigenvalue z_* and some independent Green's functions of the two-matrix model (3.2) with $g = h = 1$. The length cutoff L_{\max} restricts the number of constraints from the loop equation (3.21). The results for $\langle \text{Tr}A^2 \rangle$ and $\langle \text{Tr}A^4 \rangle$ are within the positivity bounds at higher L_{\max} in [46]. We underline the stable digits for $L_{\max} = 6, 10, 14, 18$. According to the convergence pattern, the accuracy is about 8 digits for $L_{\max} = 22$.

In Table 2-6, we summarize the results for the largest eigenvalue squared and some Green's functions at $L_{\max} = 6, 10, 14, 18, 22$. We can see that the results converge rapidly as L_{\max} increases, including the Green's functions of length-32. In the positivity bound approach, it requires more efforts to determine the Green's functions with larger lengths, so they were not presented in [46]. In our approach, it is straightforward to make predictions for the longer Greens' functions using the analytic ansatz (3.20), which covers all the independent parameters in (3.22) and thus all the single trace moments through the loop equations. Furthermore, we find that the results for the longer Green's functions also converge rather rapidly, which is related to the dominance of the contributions around the largest eigenvalues in the matrix integral.

For comparison, we summarize the rigorous bounds from the relaxation formulation of the positive bootstrap [46]:

$$0.421780275 \leq \langle \text{Tr}A^2 \rangle \leq 0.421785491, \quad 0.333339083 \leq \langle \text{Tr}A^4 \rangle \leq 0.333343006, \quad (3.49)$$

$$0.421783612 \leq \langle \text{Tr}A^2 \rangle \leq 0.421784687, \quad 0.333341358 \leq \langle \text{Tr}A^4 \rangle \leq 0.333342131, \quad (3.50)$$

where (3.49) is for $L_{\max} = 20$ and (3.50) is for $L_{\max} = 22$.¹² Our results for $\langle \text{Tr}A^2 \rangle$ and $\langle \text{Tr}A^4 \rangle$ at $L_{\max} = 14, 18$ are within the positivity bounds in [46] with $L_{\max} = 16, 20$. In fact, our $L_{\max} = 18$ results are just slightly below the lower bounds in (3.50), so they already have similar accuracy as that of the positivity bounds at the higher length cutoff $L_{\max} = 22$ in [46].

We can estimate the errors without resorting to the positivity bounds by examining how the predictions change as L_{\max} increases. The stable digits are interpreted as the reliable predictions. For example, the determinations of $\langle \text{Tr}A^2 \rangle$ are (0.4, 0.42, 0.4217, 0.421784) for $L_{\max} = 6, 10, 14, 18$. As the number of stable digits increases with L_{\max} , the errors decrease with L_{\max} , which are compatible with the positivity bounds. In Fig. 2, the convergence

¹²The parameter Λ in [46] is related to the length cutoff by $L_{\max} = 2\Lambda$.

L_{\max}	$\langle \text{Tr} A^6 \rangle$	$\langle \text{Tr} A^8 \rangle$	$\langle \text{Tr} A^6 B^2 \rangle$
6	0.3173199032	0.3544033193	0.1265726140
10	0.3234044907	0.3459107152	0.1191048039
14	0.3216387230	0.3437807762	0.1185379754
18	0.3216719741	0.3438223591	0.1185500944
22	0.3216724315	0.3438229503	0.1185502550

Table 3: The two-length trajectory bootstrap results for the independent Green’s functions of length-6, 8. Using the analytic ansatz (3.20), we also make predictions for the Green’s functions with lengths greater than the length cutoff L_{\max} for the self-consistent constraints.

L_{\max}	$\langle \text{Tr} A^{10} \rangle$	$\langle \text{Tr} A^{12} \rangle$	$\langle \text{Tr} A^{10} B^2 \rangle$
6	0.4240933591	0.5316533429	0.1691624273
10	0.3940839495	0.4686863738	0.1418586490
14	0.3912843876	0.4648134622	0.1405385457
18	0.3913404816	0.4648919176	0.1405588137
22	0.3913412639	0.4648929777	0.1405590861

Table 4: The two-length trajectory bootstrap results for the independent Green’s functions of length-10, 12.

L_{\max}	$\langle \text{Tr} A^{14} \rangle$	$\langle \text{Tr} A^{16} \rangle$	$\langle \text{Tr} A^{14} B^2 \rangle$
6	0.6892144055	0.9163798430	0.2749139529
10	0.5750990741	0.7226379655	0.2044859817
14	0.5695818537	0.7146463513	0.2016429636
18	0.5696935852	0.7148070340	0.2016768661
22	0.5696950513	0.7148090950	0.2016773715

Table 5: The two-length trajectory bootstrap results for the independent Green’s functions of length-14, 16. Our results for $\langle \text{Tr} A^{16} \rangle$ are compatible with and more accurate than the Monte Carlo result 0.7153(8) in [58].

pattern further suggests that the accuracy of $(z_*, \langle \text{Tr} A^2 \rangle, \langle \text{Tr} A^4 \rangle, \langle \text{Tr} A^2 B^2 \rangle)$ is around 8 digits for $L_{\max} = 22$.

Above, we do not present the results for the coefficients b_{k_1, k_2} of the analytic ansatz [46]. The reason is that they converge much slower than the largest eigenvalues and the Green’s functions. For example, the results for the low order coefficients at $L_{\max} = 10, 14, 18, 22$ are $b_{0,0} \approx (0.9677, 1.0287, 1.0134, 1.0149)$ and $b_{0,1} \approx (0.450, -0.183, 0.296, 0.282)$.¹³ The slow convergence rate of these expansion coefficients may be related to the uniform convergence of the eigenvalue density on the branch cut (see Fig. 3), which is different from the local convergence near the edges of the eigenvalue supports. Therefore, this is also consistent

¹³The coefficient $b_{0,2}$ seems to approach zero.

L_{\max}	$\langle \text{Tr} A^{30} \rangle$	$\langle \text{Tr} A^{32} \rangle$	$\langle \text{Tr} A^{30} B^2 \rangle$
6	9.981077191	14.51986635	3.981253675
10	5.195580912	7.113064471	1.811209013
14	5.074025608	6.932959071	1.753605763
18	5.076267533	6.936245284	1.754098130
22	5.076296208	6.936287877	1.754105280

Table 6: The two-length trajectory bootstrap results for the independent Green's functions of length-30, 32. In spite of the significant deviations at $L_{\max} = 6$, these relatively long Green's functions converge rather rapidly as L_{\max} increases. The results for $\langle \text{Tr} A^{32} \rangle$ are consistent with and more accurate than the Monte Carlo result 6.96(8) in [58].

with the rapid convergence of the Green's functions.

3.4 Eigenvalue distributions

Our conjecture (3.13) about the singularity structure of the generating functions is closely related the distributions of eigenvalues. According to the contour integration formula (3.12), we can express the one-length and two-length Green's functions as

$$\langle \text{Tr} A^n \rangle = \int_{-z_*}^{z_*} dz z^n \rho^{(1)}(z), \quad \langle \text{Tr} A^{n_1} B^{n_2} \rangle = \int_{-z_*}^{z_*} dz_1 \int_{-z_*}^{z_*} dz_2 z_1^{n_1} z_2^{n_2} \rho^{(2)}(z_1, z_2), \quad (3.51)$$

which are over the supports of the eigenvalue distributions on the real axes. The one-length eigenvalue density $\rho^{(1)}(z)$ is related to the two-length eigenvalue density $\rho^{(2)}(z_1, z_2)$ by

$$\rho^{(1)}(z_1) = \int_{-z_*}^{z_*} dz_2 \rho^{(2)}(z_1, z_2). \quad (3.52)$$

As the contours in (3.12) extract the discontinuities on the branch cuts of the generating function $R^{(2)}(z_1, z_2)$. The two-length eigenvalue density is given by

$$\rho^{(2)}(z_1, z_2) = -\frac{1}{\pi^2} \sum_{k_1+k_2 \leq k_{\max}} b_{k_1, k_2} \frac{(z_1^2 - z_*^2)^{\frac{1}{2}+k_1} (z_2^2 - z_*^2)^{\frac{1}{2}+k_2}}{\frac{(-1/2-k_1)_{k_1+1}}{(k_1+1)!} \frac{(-1/2-k_2)_{k_2+1}}{(k_2+1)!} z_*^{2(k_1+k_2+2)}}. \quad (3.53)$$

In Fig. 2, we present the eigenvalue density $\rho^{(1)}(z)$ associated with the one-length Green's functions $\langle \text{Tr} A^n \rangle$ for the length cutoff $L_{\max} = 6, 10, 14, 18, 22$, which converges rapidly as L_{\max} increases. Our results for the eigenvalue distribution confirm and are more accurate than the Monte Carlo results in [58]. In Fig. 3, we further show that the convergence of $\rho^{(1)}(z)$ is uniform on the support of the eigenvalue distribution.¹⁴ Using the two-length eigenvalue density $\rho^{(2)}(z_1, z_2)$, we can also compute the generalized one-length eigenvalue densities, such as $\rho_{B^2}^{(1)}(z)$, $\rho_{B^4}^{(1)}(z)$, $\rho_{B^6}^{(1)}(z)$. They are associated with the generalized resolvent $R_{\mathcal{O}}(z)$ in (3.15) and the one-length Green's function

$$\langle \text{Tr} A^n \mathcal{O} \rangle = \int_{-z_*}^{z_*} dz z^n \rho_{\mathcal{O}}^{(1)}(z). \quad (3.54)$$

¹⁴Our ansatzes are can viewed as rational approximations of the eigenvalue distributions.

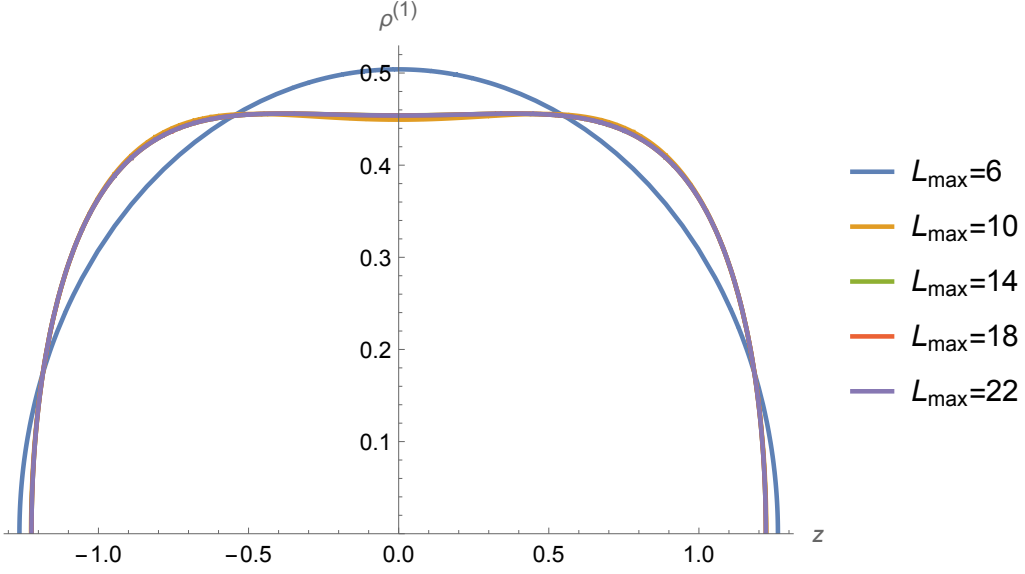


Figure 2: The one-length eigenvalue density $\rho^{(1)}(z)$ of the two-matrix model (3.2) with $g = h = 1$, which encodes the information of the one-length Green's functions $\langle \text{Tr} A^n \rangle$. We use (3.52), (3.53) and the one-cut solutions at $L_{\max} = 6, 10, 14, 18, 22$ to evaluate $\rho^{(1)}(z)$. As our results converge rapidly, the curves for $L_{\max} = 14, 18, 22$ are indistinguishable from each other. The eigenvalue distribution is consistent with and more accurate than the Monte Carlo results in [58].

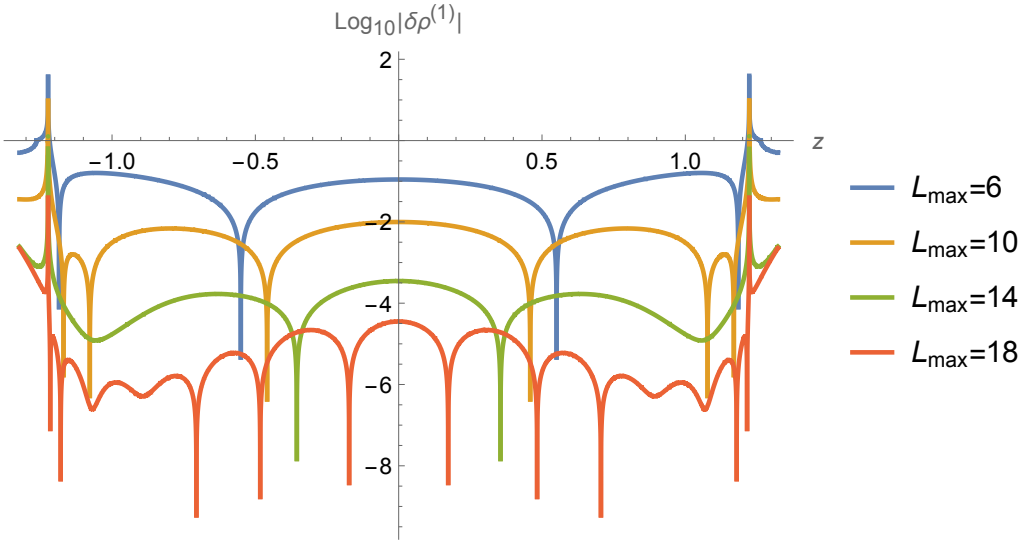


Figure 3: The relative error of the eigenvalue density $\delta\rho^{(1)} = \rho^{(1)}/\rho_{\text{ref}}^{(1)} - 1$ for various L_{\max} . We choose the $L_{\max} = 22$ solution as the reference density $\rho_{\text{ref}}^{(1)}$. As L_{\max} increases, the approximate density improves uniformly on the support of the eigenvalue distribution.

where $\rho_{\mathcal{O}}^{(1)}(z)$ with $\mathcal{O} = B^2, B^4, B^6, \dots$ are given by

$$\rho_{B^{n_2}}^{(1)}(z_1) = \int_{-z_*}^{z_*} dz_2 z_2^{n_2} \rho^{(2)}(z_1, z_2). \quad (3.55)$$

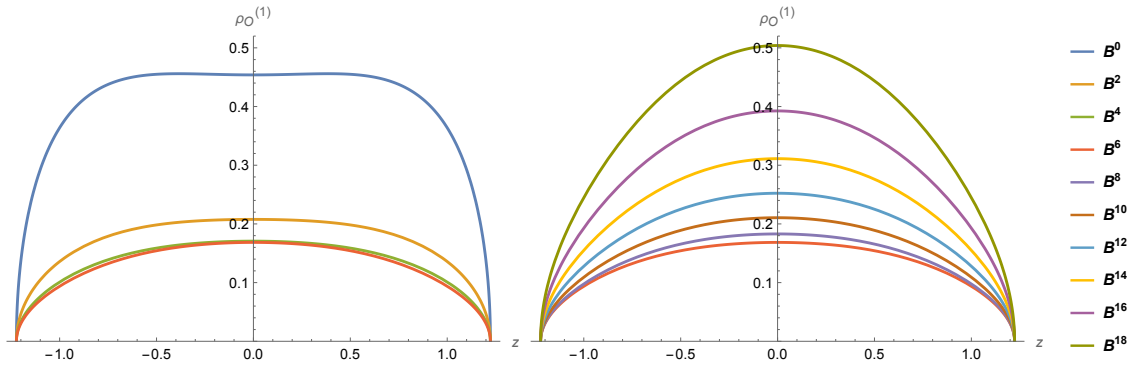


Figure 4: The generalized one-length eigenvalue densities $\rho_{\mathcal{O}}^{(1)}(z)$ of the two-matrix model (3.2) with $g = h = 1$, which are associated with the generalized one-length Green's functions $\langle \text{Tr} A^n \mathcal{O} \rangle$, where $\mathcal{O} = B^0, B^2, \dots, B^{18}$. We evaluate them using (3.53), (3.55) and the one-cut solution at $L_{\max} = 22$.

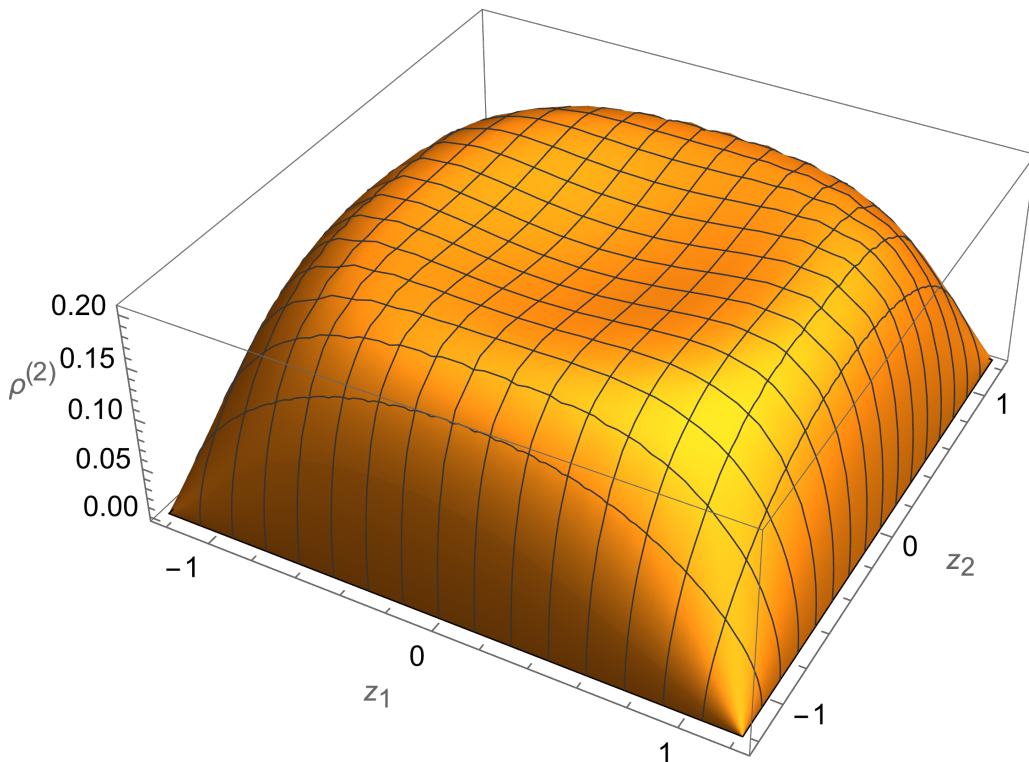


Figure 5: The two-length eigenvalue density $\rho^{(2)}(z_1, z_2)$ of the two-matrix model (3.2) with $g = h = 1$. The density of eigenvalues is related to the two-length Green's functions $\langle \text{Tr} A^{n_1} B^{n_2} \rangle$. We use (3.53) and the 1-cut solution at $L_{\max} = 22$ to evaluate $\rho^{(2)}(z_1, z_2)$.

The standard one-length eigenvalue density in (3.52) corresponds to the case of $\mathcal{O} = B^0$. In Fig. 4, we present the results for $\rho_{\mathcal{O}}^{(1)}(z)$ with $\mathcal{O} = B^0, B^2, \dots, B^{18}$. As the power n grows, we find that $\rho_{B^n}^{(1)}(0)$ decreases for $n \leq 6$ and increases for $n \geq 6$.

The two-length eigenvalue density does not take a simple factorized form due to the

nontrivial angle dependence in the matrix integrals. In Fig. 5, we present the two-length eigenvalue density $\rho^{(2)}(z_1, z_2)$ associated with the two-length Green's functions $\langle \text{Tr} A^{n_1} B^{n_2} \rangle$ for $L_{\max} = 22$.

As a consistency check, we verify that the integrals in (3.51) and (3.54) with the eigenvalue density (3.53) reproduce the results for the independent Green's functions in Table 2-6.

4 Symmetry breaking solutions

Above, we assume the solutions of the two-matrix model are invariant under the \mathbb{Z}_2 transformations

$$A \leftrightarrow -A, \quad B \leftrightarrow -B, \quad (4.1)$$

so the Green's functions with an odd number of A or B should vanish. If the coefficients of the quadratic terms are negative, we have a double well potential. It is natural to consider symmetry breaking solutions, as the tunneling effect is suppressed by the thermodynamic-like large- N limit. To capture the symmetry breaking phenomena, we need to extend the symmetric one-cut ansatzes to more complicated forms.

In Sec. 4.1, we will briefly review the symmetry breaking solutions in the one-matrix model, which provides natural building blocks for the two-matrix ansatzes. In Sec. 4.2, we will use more complicated ansatzes to study the solutions with spontaneously broken symmetries in the two-matrix model.

4.1 One-matrix model

Let us consider the potential with a negative coefficient for the quadratic term

$$V(M) = -\frac{1}{2}M^2 + \frac{g}{4}M^4, \quad (4.2)$$

where $g > 0$. We refer to [10, 46] for discussions with more emphasis on the positivity constraints. Some main features of this one-matrix model extend to the two-matrix version with $\text{Tr}[A, B]^2$ interaction.

As in (2.5), we can consider the one-cut solutions. If we do not impose the \mathbb{Z}_2 symmetry, the one-cut ansatz for the resolvent reads

$$R^{(\text{one-cut})}(z) = \sum_{k=0}^{k_{\max}} a_k z^k \sqrt{(z - z_{*,1})(z - z_{*,2})} + \text{regular}, \quad (4.3)$$

where $k_{\max} = 2$ for the quartic potential (4.2). As in (2.6) and (2.7), we can extract the single trace moments from the large z expansion of the singular part of the resolvent. Then we can determine the free parameters by the loop equations

$$-G_{n+1} + gG_{n+3} = \sum_{p=0}^{n-1} G_p G_{n-p-1}. \quad (4.4)$$

For example, we obtain $a_2 = -g/2$. We have two types of one-cut solutions:

- $\langle \text{Tr}M \rangle = 0$

In this case, the single trace moment $\langle \text{Tr}M^n \rangle$ vanishes if n is an odd number, so the \mathbb{Z}_2 symmetry is preserved. As the loop equations require that $a_1 = 0$ and $z_1 = -z_2$, the solution takes the form in (2.5). The other parameters can be expressed in terms of $z_*^2 = z_1^2 = z_2^2$, such as

$$\langle \text{Tr}M^2 \rangle = \left(\frac{1}{3} + \frac{1}{36g} \right) z_*^2 + \frac{1}{9g}, \quad a_0 = \frac{(z_*^2)^2}{512} - \left(\frac{g}{4} + \frac{1}{384g} \right) z_*^2 + \frac{1}{2} - \frac{1}{96g}. \quad (4.5)$$

Since z_*^2 satisfies the quadratic equation $3g(z_*^2)^2 - 4z_*^2 - 16 = 0$, we have two solutions

$$z_{*,\pm}^2 = \frac{2}{3g} \left(1 \pm \sqrt{1 + 12g} \right). \quad (4.6)$$

The branch points associated with the $z_{*,-}^2$ solution are on the imaginary axis. Since $z_{*,+}^2$ is positive, the corresponding eigenvalue distribution is supported on the real axis. The eigenvalue density of the $z_{*,+}^2$ solution is positive on the support for $g \geq 1/4$, but it becomes negative around $z = 0$ for $g < 1/4$.¹⁵

- $|\langle \text{Tr}M \rangle| > 0$

In this case, the \mathbb{Z}_2 symmetry is spontaneously broken. The symmetry breaking solution can be parametrized by the order parameter $\langle \text{Tr}M \rangle$. For example, we have

$$\langle \text{Tr}M^2 \rangle = \frac{1}{3g(1 + 60g)} \left(3 + 52g + 125g^2 \langle \text{Tr}M \rangle^2 \right), \quad (4.7)$$

which is positive for the real solutions of $\langle \text{Tr}M \rangle$. One can show that $\langle \text{Tr}M \rangle^2$ satisfies the quadratic equation

$$28125g^4 x^2 - 8g(2 + 75g + 4500g^2)x + 16(1 + 12g)^3 = 0. \quad (4.8)$$

The explicit one-cut solutions for $\langle \text{Tr}M \rangle_{\pm}^2$ are

$$\langle \text{Tr}M \rangle_{\pm}^2 = \frac{4}{28125g^3} \left(2 + 75g + 4500g^2 \pm 2(1 + 60g)(1 - 15g)^{3/2} \right), \quad (4.9)$$

which are positive real for $0 < g \leq \frac{1}{15}$. For $g > \frac{1}{15}$, the one-cut solutions in (4.9) are a pair of complex conjugates. As g decreases, they meet at $g = \frac{1}{15}$ and then become real solutions for $0 < g \leq \frac{1}{15}$. Although the corresponding branch points of the resolvents are all located on the real axis, those of the $\langle \text{Tr}M \rangle_+$ solution have opposite signs for $0 < g < \frac{1}{20}$. Furthermore, the eigenvalue density of the $\langle \text{Tr}M \rangle_+$ solution is negative at small $|z|$, while that of $\langle \text{Tr}M \rangle_-$ solution is always positive. Therefore, $\langle \text{Tr}M \rangle_-$ is more physical than $\langle \text{Tr}M \rangle_+$ in the range $0 < g \leq \frac{1}{15}$.

¹⁵We thank Zechuan Zheng for clarifying this point.

For $0 < g < 1/4$, we should introduce a more complicated ansatz in order to capture the generic \mathbb{Z}_2 symmetry breaking behavior. We consider the next-to-minimally singular solutions, i.e. the two-cut solutions. The corresponding ansatz for the resolvent reads

$$R^{(\text{two-cut})}(z) = \sum_{k=0}^{k_{\max}} a_k z^k \sqrt{(z - z_{*,1})(z - z_{*,2})(z - z_{*,3})(z - z_{*,4})} + \text{regular}, \quad (4.10)$$

where $k_{\max} = 1$ for the quartic potential (4.2). The two-cut solutions can be parametrized by the symmetry breaking order parameter $\langle \text{Tr}M \rangle$. The more physical solutions have eigenvalues supported on the real axis, then we assume $z_{*,1} \geq z_{*,2} \geq z_{*,3} \geq z_{*,4}$. Although the building blocks of (4.10) do not lead to simple analytic expressions, we can still extract the single trace moments from the large z expansion of the singular part, as in (2.6) and (2.7). Then we can use the loop equations to solve for the free parameters, such as $a_1 = -g/2$.

Let us first examine the \mathbb{Z}_2 symmetric limit of the two-cut solutions

$$z_{*,1} = -z_{*,4}, \quad z_{*,2} = -z_{*,3}, \quad a_0 = 0. \quad (4.11)$$

In this special case, the eigenvalues are symmetrically distributed near the two minima of the effective potential for the matrix eigenvalues. The \mathbb{Z}_2 symmetric two-cut resolvent takes a simple form

$$R^{(\text{two-cut, s})}(z) = a_1 z \sqrt{(z^2 - z_{*,1}^2)(z^2 - z_{*,2}^2)} + \text{regular}, \quad (4.12)$$

which implies $\langle \text{Tr}M \rangle = 0$. The remaining parameters can be determined by the loop equations. We have

$$R^{(\text{two-cut, s})}(z) = -\frac{g}{2} z \sqrt{\left(z^2 - \frac{1 - 2\sqrt{g}}{g}\right) \left(z^2 - \frac{1 + 2\sqrt{g}}{g}\right)} + \text{regular}, \quad (4.13)$$

which implies $\langle \text{Tr}M^2 \rangle = \frac{1}{g}$. For $0 < g < 1/4$, the eigenvalue distribution is supported on the real axis with positive eigenvalue density. For $g = 1/4$, two branch points approach zero and we obtain the symmetric one-cut solution associate with $z_{*,+}^2$ in (4.6). For $g > 1/4$, we have $1 - 2\sqrt{g} < 0$, so the two branch points are a pair of complex conjugates on the imaginary axis.

After examining the special cases, we consider the generic two-cut solution in (4.10). In the limit $\langle \text{Tr}M \rangle \rightarrow 0$, the more physical branch of solution should reduce to the \mathbb{Z}_2 symmetric one-cut solution (4.6) for $g \geq 1/4$ and the \mathbb{Z}_2 symmetric two-cut solution (4.13) for $0 < g < 1/4$. For a given $\langle \text{Tr}M \rangle$, we obtain a quintic equation for $\langle \text{Tr}M^2 \rangle$, so there are five branches of solutions. The other parameters can be expressed in terms of $\langle \text{Tr}M^2 \rangle$. For $g = \frac{1}{30}$, the explicit algebraic equation for $G_1 = \langle \text{Tr}M \rangle$ and $G_2 = \langle \text{Tr}M^2 \rangle$ reads

$$\begin{aligned} G_2^5 - \frac{410}{3} G_2^4 + \frac{5}{9} (10696 - 75G_1^2) G_2^3 + \frac{250}{27} (-8296 + 513G_1^2) G_2^2 \\ + \frac{25}{324} (-2085824 - 2566320G_1^2 + 3375G_1^4) G_2 \\ + \frac{25}{1944} (-6094080 + 218680896G_1^2 - 681900G_1^4 + 625G_1^6) = 0. \end{aligned} \quad (4.14)$$

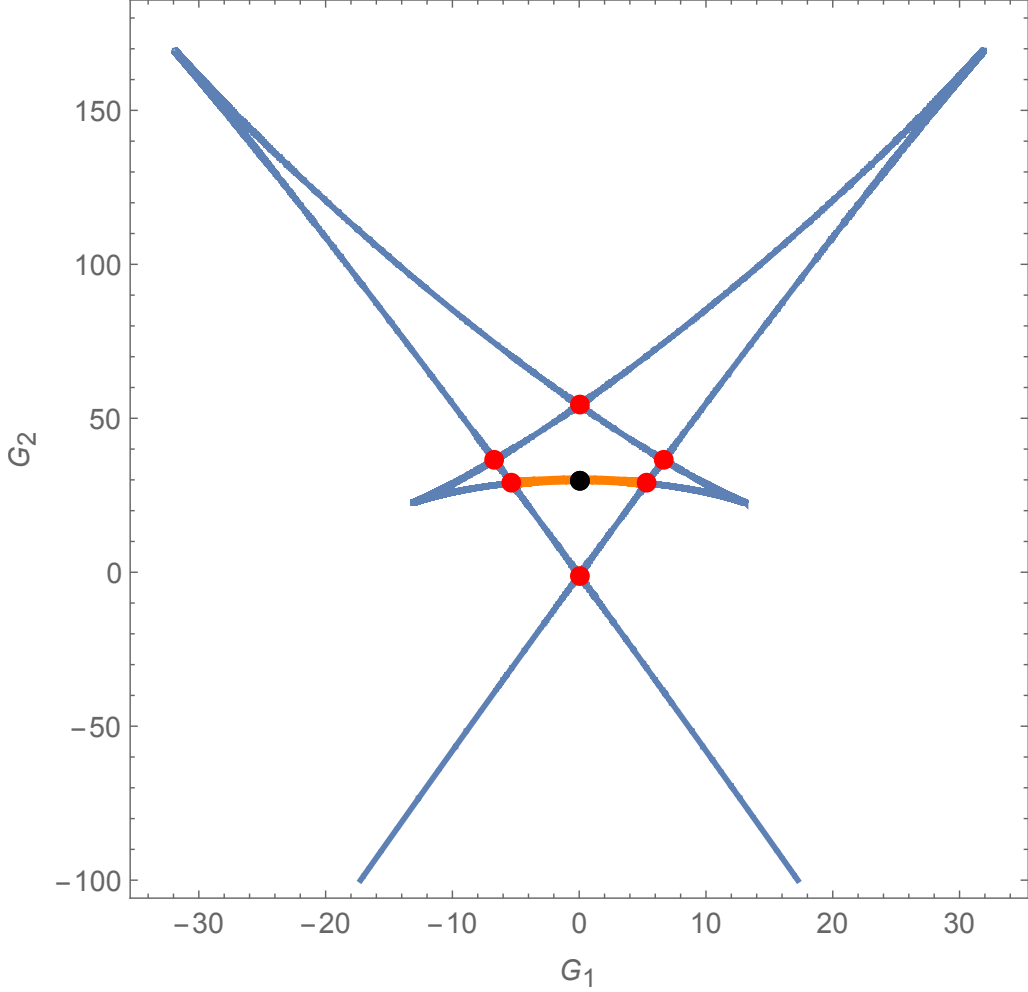


Figure 6: The two-cut solutions of the large- N one-matrix model with the potential $V(M) = -\frac{1}{2}M^2 + \frac{g}{4}M^4$, where $g = \frac{1}{30}$, $G_1 = \langle \text{Tr}M \rangle$ and $G_2 = \langle \text{Tr}M^2 \rangle$. The red dots represent the one-cut solutions (4.6) and (4.9), which are located at the intersection points of the two-cut solutions. The black dot indicates the \mathbb{Z}_2 symmetric two-cut solution (4.13). The two-cut solution with positive density of eigenvalues supported on the real axis is denoted by the orange curve, whose endpoints are the one-cut solutions at $(G_1, G_2) \approx (\pm 5.32, 28.9)$.

The generic g version of this algebraic equation can be found in [46]. In Fig. 6, we present the real solutions of (G_1, G_2) from the two-cut ansatz (4.10) with $g = \frac{1}{30}$. We notice that

- The one-cut solutions can be connected by two-cut solutions.
- The one-cut solutions emerge at the intersection points of the two-cut solutions.

As G_1 changes, some two-cut solutions for G_2 may collide and become a pair of complex conjugates, so they annihilate each other from the perspective of real solutions. We do not find any one-cut solutions associated with these annihilations. As we increase g , the two symmetry breaking one-cut solutions meet at $g = \frac{1}{15}$ and become a pair of complex

conjugates for $g > \frac{1}{15}$. For $\frac{1}{15} < g < \frac{1}{4}$, the more physical branch of real solution cannot reach the one-cut limit because the annihilations happen at smaller $|\text{Re}(G_1)|$. If we further increase g , the more physical branch of solution shrinks to a point at $g = \frac{1}{4}$. For $g \geq \frac{1}{4}$, the more physical solution is given by the \mathbb{Z}_2 symmetric one-cut solution associated with $z_{*,+}^2$ in (4.6).

Using the analytic ansatzes for the singular part of the resolvent, we are able to study the various types of one-cut solutions and two-cut solutions. Although some solutions are more physical than the others, the intersections or collisions of the less physical solutions help us to understand better the more physical ones, such as their range and evolution behavior as the coupling constant g changes. Below, we will apply this approach to the more complicated two matrix model with $\text{Tr}[A, B]^2$ interaction.

4.2 Two-matrix model

To the study the symmetry breaking solutions of the two-matrix model, we consider the following potential

$$V(A, B) = -\frac{1}{2}A^2 + \frac{g}{4}A^4 - \frac{1}{2}B^2 + \frac{g}{4}B^4 - \frac{h}{2}[A, B]^2. \quad (4.15)$$

For $h = 0$, we have two decoupled one-matrix models, which allow for symmetric breaking solutions for $0 < g < \frac{1}{4}$. Below, we focus on the case of $g = \frac{1}{30}, h = \frac{1}{15}$, which is not solvable by the known analytic methods. If the \mathbb{Z}_2 symmetry is spontaneously broken, there are more independent Green's functions. For $L_{\max} < 16$, we can again choose the two-length Green's functions as the independent ones, such as those in (3.22) and

$$G_1, \quad G_{1,1}, \quad G_{1,2}, \quad G_5, \quad G_7, \quad G_{1,7}, \quad G_{1,11}, \quad G_{13}, \quad G_{1,14}. \quad (4.16)$$

We assume that the \mathbb{Z}_2 symmetry $A \leftrightarrow B$ is unbroken, so we have $G_{n_1, n_2} = G_{n_2, n_1}$. We also use the simplified notation $G_n = G_{0, n}$. Below we mainly consider $L_{\max} \leq 8$. The loop equations imply some self-consistent constraints for the two-length Green's functions. Some explicit examples are

$$G_{0,3} = -30G_{0,1}, \quad G_{1,3} = G_{1,1}, \quad G_{2,3} = 30G_{1,2}, \quad (4.17)$$

$$G_{1,4} = -450G_{0,1} + 30G_{1,2} + \frac{1}{2}G_{0,5}, \quad (4.18)$$

$$G_{2,4} = \frac{5}{2}G_{0,1}^2 - 70G_{0,2} + 30G_{2,2} - 5G_{0,4} + \frac{1}{4}G_{0,6} - 75, \quad (4.19)$$

$$G_{1,5} = G_{0,2}G_{1,1} + G_{0,1}G_{1,2} + 900G_{1,1}, \quad G_{3,3} = 900G_{1,1}, \quad (4.20)$$

$$G_{4,4} = \frac{1}{11} \left(600G_{0,1}^2 + 80G_{1,1}^2 + 175G_{0,2}^2 - 38250G_{0,2} + 15865G_{2,2} - 5360G_{0,4} + 190G_{0,6} + G_{0,8} - 36000 \right) + 25G_{1,2}G_{0,1} - \frac{13G_{2,6}}{22}. \quad (4.21)$$

For symmetric solutions, the nontrivial constraints are associated with (4.19) and (4.21). We do not present the length-7 and other length-8 constraints as they are not used below. As in the case of the one-matrix model, the symmetry breaking solutions of the two-cut type can be parametrized by the order parameter

$$G_1 = \langle \text{Tr} A \rangle = \langle \text{Tr} B \rangle . \quad (4.22)$$

As a generalization of the (4.10), we introduce to a two-cut ansatz for the two-length generating function

$$R^{(2)}(z_1, z_2) = \sum_{k_1=0}^{k_{\max}} \sum_{k_2=0}^{k_{\max}-k_1} a_{k_1, k_2} \prod_{j=1,2} z_j^{k_j} \sqrt{(z_j - z_{*,1})(z_j - z_{*,2})(z_j - z_{*,3})(z_j - z_{*,4})} + \text{regular} . \quad (4.23)$$

The support for the eigenvalue distribution is encoded in the locations of the branch points. There are 4 different branch points in (4.23).

In the one-cut limit, two branch points meet $z_{*,3} - z_{*,4} \rightarrow 0$ and become a regular point located at $z_{*,3}$. Accordingly, the one-cut ansatz for the two-length generating function reads

$$R^{(2)}(z_1, z_2) = \sum_{k_1=0}^{k_{\max}} \sum_{k_2=0}^{k_{\max}-k_1} a_{k_1, k_2} \prod_{j=1,2} z_j^{k_j} (z_j - z_{*,3}) \sqrt{(z_j - z_{*,1})(z_j - z_{*,2})} + \text{regular} , \quad (4.24)$$

where $(z_{*,1}, z_{*,2})$ denote the locations of the two branch points. For $g = \frac{1}{30}$, we expect that $G_1 \neq 0$ for the more physical solutions as in the case of the one-matrix model. For $k_{\max} = 0$, we have 4 parameters $(z_{*,1}, z_{*,2}, z_{*,3}, a_{0,0})$, so we need 4 equations. The first equation is again the normalization condition $G_{0,0} = 1$. If we impose the first constraint in (4.17), then the second and third ones in (4.17) are automatically satisfied. Then we can make use of the two constraints in (4.18) and (4.19). We obtain 30 solutions and 20 of them are real solutions. For the positivity of the eigenvalue density, we further impose that $(z_{*,3} - z_{*,1})(z_{*,3} - z_{*,2}) > 0$, which selects two pairs of solutions. If the eigenvalues are distributed around a local minimum of the effective potential, the solution should satisfy $z_{*,1} z_{*,2} > 0$. In the end, we find only one pair of solutions

$$(G_1, G_2, z_{*,1}, z_{*,2}) \approx (\pm 5.3293, 28.9401, \pm 6.6627, \pm 3.6454) , \quad (4.25)$$

with $z_{*,3} \approx \pm 1.9079$ and $a_{0,0} \approx 0.073275$. It is also natural to replace (4.18) with (4.21), as the latter one does not vanish automatically for the symmetric solution. In this case, we have 56 solutions. After imposing the same additional requirements, we again obtain only one pair of solutions

$$(G_1, G_2, z_{*,1}, z_{*,2}) \approx (\pm 5.3292, 28.9392, \pm 6.6641, \pm 3.6474) , \quad (4.26)$$

with $z_{*,3} \approx \pm 1.8770$ and $a_{0,0} \approx 0.071883$. For $k_{\max} = 2$, there are 3 more free parameters $(a_{0,1}, a_{0,2}, a_{1,1})$, so we take into account the self-consistent constraints in (4.17), (4.18),

(4.19), together with the normalization condition $G_{0,0} = 1$ and the first constraint in (4.20). As the number of solutions increases significantly, we use the efficient package `HomotopyContinuation.jl` to solve the systems of polynomial equations here and below. Then we extract two pairs of solutions by the same requirements as above

$$\begin{aligned} (G_1, G_2, z_{*,1}, z_{*,2}) &\approx (\pm 5.32892, 28.93747, \pm 6.68471, \pm 3.14985), \\ &(\pm 5.32897, 28.93779, \pm 6.68441, \pm 3.58664). \end{aligned} \quad (4.27)$$

For a different combination of the length-6 constraints, we do not find any real solution. It is also natural to replace the first constraint in (4.20) with (4.21), as the latter is nontrivial for the symmetric solution. Then the solutions are

$$\begin{aligned} (G_1, G_2, z_{*,1}, z_{*,2}) &\approx (\pm 5.32878, 28.93663, \pm 6.68555, \pm 3.50902), \\ &(\pm 5.32880, 28.93672, \pm 6.68738, \pm 3.18846), \\ &(\pm 5.32891, 28.93741, \pm 6.68819, \pm 3.57615). \end{aligned} \quad (4.28)$$

As in the case of the one-matrix model with $g = \frac{1}{30}$, these one-cut solutions should be related to the endpoints of the more physical branch of symmetry breaking solutions. The estimates $(G_1, G_2) \approx (\pm 5.329, 28.937)$ are well consistent with the edges of the positivity bounds obtained for a much higher length cutoff $L_{\max} = 16$ in [46].

Another special limit is the \mathbb{Z}_2 symmetric solution

$$z_{*,1} = -z_{*,4}, \quad z_{*,2} = -z_{*,3}, \quad (4.29)$$

and a_{k_1, k_2} vanishes if k_1 or k_2 is an even integer. The lowest cutoff for the \mathbb{Z}_2 symmetric ansatz is $k_{\max} = 2$. The corresponding two-cut ansatz reads

$$R^{(2)}(z_1, z_2) = a_{1,1} z_1 z_2 \sqrt{(z_1^2 - z_{*,1}^2)(z_1^2 - z_{*,2}^2)} \sqrt{(z_2^2 - z_{*,1}^2)(z_2^2 - z_{*,2}^2)} + \text{regular}. \quad (4.30)$$

which contains 3 free parameters $(a_{1,1}, z_{*,1}^2, z_{*,2}^2)$. They can be determined by the normalization condition $G_{0,0} = 1$ and the length-6,8 constraints in (4.19), (4.21). We find 6 solutions, but only one of them is real

$$(G_2, G_4, G_{2,2}, z_{*,1}^2, z_{*,2}^2) \approx (29.7461, 902.788, 884.828, 6.1824^2, 4.6119^2). \quad (4.31)$$

The approximate solution for G_2 is also consistent with the upper bound from positivity constraints for $L_{\max} = 16$ in [46].

After studying two special limits, we consider the generic symmetry breaking solution. According to the one-matrix model results, one may expect that the more physical branch of two-cut solution should interpolate between the asymmetric one-cut and the symmetric two-cut solutions, such as those in (4.28) and (4.31) for $k_{\max} = 2$. However, as the numbers of solutions do not match, it is impossible that all the asymmetric one-cut solutions are smoothly connected to the symmetric two-cut solutions. In Fig. 7, we present the real solutions of the two-cut ansatz in the relevant region.¹⁶ For a given G_1 , the free parameters

¹⁶There are many real solutions that are not in this region.

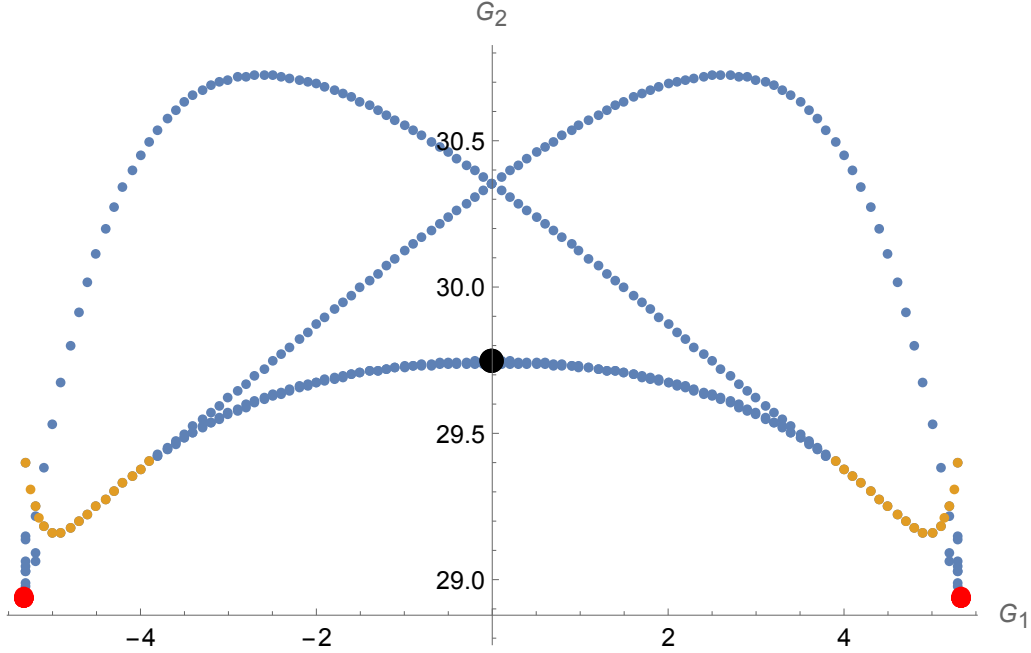


Figure 7: The two-cut solutions of the large- N two-matrix model with the potential $V(A, B) = -\frac{1}{2}A^2 + \frac{g}{4}A^4 - \frac{1}{2}B^2 + \frac{g}{4}B^4 - \frac{h}{2}[A, B]^2$, where $g = \frac{1}{30}, h = \frac{1}{15}$, $G_1 = \langle \text{Tr} A \rangle$ and $G_2 = \langle \text{Tr} A^2 \rangle$. We use (4.23) with $k_{\max} = 2$ as the two-cut ansatz for the two-length generating function. We consider $G_1 = \pm \frac{k}{10}$ with $k = 10^{-5}$ and $k = 1, 2, \dots, 52, 53$. For $|G_1| \leq 3.8$, the lowest branch is associated with two nearly degenerate solutions. The one connected to the symmetric two-cut solution annihilates with the middle branch at $G_1 \approx \pm 3.9$. For $|G_1| \geq 3.9$, the lower branch and its continuation is represented by the orange dots. The pairs of asymmetric one-cut solutions in (4.25), (4.26), (4.27), (4.28) are denoted by red dots, but they are not distinguishable. The symmetric two-cut solution in (4.31) is indicated by the black dot.

are determined by the constraint associated with G_1 , the normalization condition $G_0 = 1$, and the self-consistent constraints in (4.17), (4.18), (4.19), (4.21). In Fig. 7, there are two nearly degenerate solutions in the lowest branch for $|G_1| \leq 3.8$ and then three nearly degenerate solutions at $(G_1, G_2) \approx (\pm 3.9, 29.4)$.¹⁷ As $|G_1|$ increases, the continuation of the symmetric solution and the middle branch meet and become a pair of complex conjugates. In Fig. 8, we present the continuations of these three solutions in the complex space. The annihilated solutions are weakly complex in $3.9 \leq |G_1| \leq 5.27$ and become real again for $|G_1| \geq 5.28$. For $G_1 = \pm 5.329$, the lowest branch gives $G_2 \approx 28.9407$, which is slightly above the asymmetric one-cut solutions in (4.28). We also find considerably more

¹⁷For $G_1 = \pm 3.88$, the three nearly degenerate solutions are $G_2 \approx 29.40713, 29.40766, 29.40774$, which are consistent with the Monte Carlo results $G_1 = \pm 3.88(2), G_2 = 29.41(4)$ in [58], as well as the upper limit of the positivity bounds in [46]. The Monte Carlo results were obtained from the starting matrix $A, B = I$. It is not clear if the fact that the corresponding results are close to the collision point at $G_1 \approx 3.9$ is a coincidence or related to the collision phenomena.

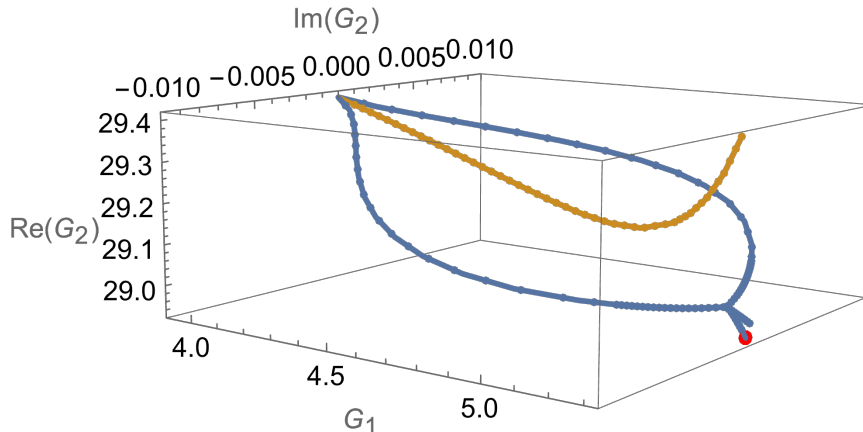


Figure 8: Some two-cut solutions of the two-matrix model in the complex space. The real solution in orange is the same as the one in Fig. 7. The two solutions in blue meet at $|G_1| \approx 3.9$ and become a pair of complex conjugates as $|G_1|$ increases. They meet again at around $|G_1| = 5.27$ and become real solutions. At $|G_1| \approx 5.33$, the lowest branch is close to the asymmetric one-cut solutions denoted by nearly degenerate red dots.

real two-cut solutions around the asymmetric one-cut solutions. It is not clear to us if the small imaginary parts are artifacts of our crude approximation scheme. To clarify this point, we need to study the cases of $k_{\max} > 2$, but they are computationally more expensive and left for the future.

5 Discussion

In conclusion, we have demonstrated the effectiveness of the analytic trajectory bootstrap method in solving the large N two-matrix model with $\text{Tr}[A, B]^2$ interaction and quartic potentials. Our results provide highly accurate solutions (see e.g. Table 2) and offer new insights into the behavior of eigenvalue distributions and symmetry-breaking solutions. While not relying on positivity requirements, our method exceeded the accuracy of the relaxation bootstrap by fully utilizing non-linear loop equations. The analytic trajectory bootstrap method thus proves to be a powerful tool for efficiently solving large N matrix models, providing highly accurate solutions and paving the way for further investigations into more complex scenarios.

In Sec. 3.4, we discuss the distributions of eigenvalues for one-length and two-length Green's functions. From the matrix integral perspective, the angular dependence has been integrated out and we present the results for the one-length and two-length eigenvalue densities. Our approach and results may shed light on a better understanding of these angular integrals. For $g = 0$, the two-matrix model is analytically solvable [66, 67], even though there are infinitely many base moments, i.e., $\langle \text{Tr} A^{2j} \rangle$ with $j = 0, 1, 2, \dots$. For generic parameters $g \neq 0, h \neq 0$, the additional base moments for the symmetric solution are $\langle \text{Tr} A^{4j-2} B^2 \rangle$ with $j = 1, 2, \dots$, so the number of free parameters is just about 1.5 times that of the $g = 0$ case. Given the rapid convergence and low computational cost in

our study, it is possible that the two-matrix model (3.2) is analytically solvable in some novel sense or by some novel methods for $g = h = 1$ or, more generally, $g \neq 0, h \neq 0$.

In Sec. 2 and Sec. 3, we mainly focus on the real solutions, but the analytic trajectory bootstrap method naturally applies to the complex cases, which may not be studied by the positivity-based bootstrap methods. For instance, some weakly complex solutions are examined in Sec. 4. In general, the dimension of the search space will be doubled, as a complex number is specified by two real numbers, the real and imaginary parts. From the algebraic geometry perspective, there are no essential differences between the real and complex solutions, i.e. we are not able to directly extract to the real solutions. We first find out all the solutions in the complex parameter space and then select the real solutions with vanishing imaginary parts. It would be useful to develop a systematic homotopy-continuation approach, so we can study the continuous families of solutions from some special limits with higher symmetries or/and simpler singularity structure, which are easier to solve more accurately. In quantum field theory, a similar strategy is to first study the fixed points of renormalization group flow and then the flow between them. The fixed points as special limits can have higher symmetries, such as scale or conformal invariance, and simpler analytic structure. It would also be interesting to revisit the conformal bootstrap [68–70] by expanding the correlators in terms of more sophisticated building blocks that can capture both the global analytic structure and the leading singularities in a systematic manner.¹⁸

We plan to apply the analytic trajectory bootstrap to more complicated multi-matrix models, especially those with supersymmetries. Some prominent targets are the Ishibashi-Kawai-Kitazawa-Tsuchiya matrix model [71], the Banks-Fischler-Shenker-Susskind matrix quantum mechanics [72], and the Berenstein-Maldacena-Nastase deformation [73]. In lattice gauge theories, it is natural to consider the large length limit, as the Wilson loop serves as a nonlocal order operator for confinement. In a deconfined phase, the expectation value of the large Wilson loop is expected to obey the perimeter law. In a confined phase, the leading behavior of the large Wilson loop should follow the area law due to the linearly growing potential $V(r) \sim \sigma r$ between static charges, where σ is the string tension. Here the confining flux tube furnishes a semi-classical picture for the large length limit. It would be fascinating to bootstrap the phases of gauge theories by the large length expansion and the analytic continuation in the loop length, which give rise to various types of trajectories of Wilson loops. The diverse choices for the loop configurations should lead to even more intricate intersections of the analytic trajectories than the case of the two-matrix model in Fig. 1. Another natural type of observables is the expectation value of a large power of identical plaquettes, i.e. the large multiplicity limit.

Acknowledgments

I would like to thank Zechuan Zheng for helpful discussions. This work was supported by the Natural Science Foundation of China (Grant No. 12205386) and the Guangzhou Municipal Science and Technology Project (Grant No. 2023A04J0006).

¹⁸The conformal correlators are analogous to the generating functions of the matrix models. See [65] for a recent conformal bootstrap study of the 3D Ising CFT, which shares the same spirit as the present work.

A Analytic ansatz from matrix integrals

For the one-matrix model, a \mathbb{Z}_2 -symmetric 1-cut solution gives

$$G_n = \langle \text{Tr } M^n \rangle = \int_{-z_*}^{z_*} dz z^n \rho(z), \quad (\text{A.1})$$

where the density of the eigenvalue distribution is given by

$$\rho(z) = -\frac{1}{2\pi i} [R(z+i0) - R(z-i0)] = -\frac{1}{\pi i} \sum_{k=0}^{k_{\max}} a_k (z^2 - z_*^2)^{\frac{1}{2}+k}. \quad (\text{A.2})$$

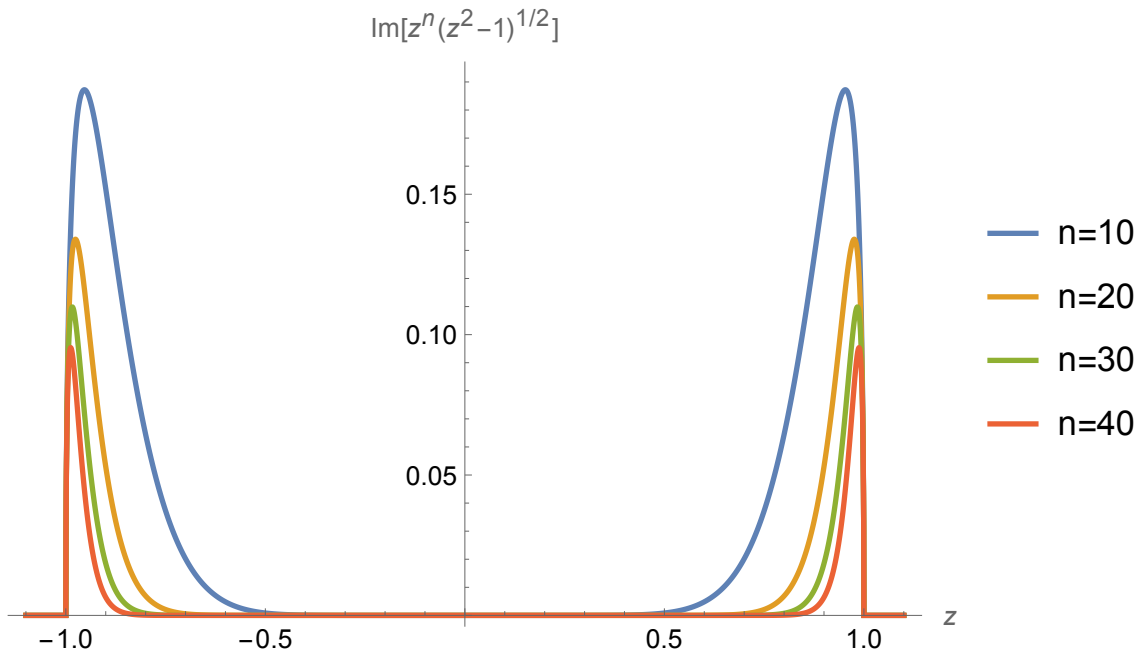


Figure 9: As n increases, the dominant contributions in (A.3) localize near the boundary of the integration interval. At large n , the maxima of $\text{Im}[z^n(z^2 - 1)^{1/2}]$ exhibit an $n^{-1/2}$ decay, while the widths are proportional to n^{-1} . Here we choose $z_*^2 = 1$, so the z_*^{n+2} dependence is not visible.

According to the basic integral

$$\int_{-z_*}^{z_*} dz z^n (z^2 - z_*^2)^{\frac{1}{2}+k} = -\pi i \frac{1 + (-1)^n}{2} \frac{(-1/2 - k)_{k+1}}{(k+1)!} z_*^{2(k+1)} \frac{(1/2)_{n/2}}{(k+2)_{n/2}} z_*^n, \quad (\text{A.3})$$

we obtain the analytic ansatz (2.7)

$$G_n = \frac{1 + (-1)^n}{2} \sum_{k=0}^{k_{\max}} \left(a_k \frac{(-1/2 - k)_{k+1}}{(k+1)!} z_*^{2(k+1)} \right) \frac{(1/2)_{n/2}}{(k+2)_{n/2}} z_*^n. \quad (\text{A.4})$$

At large n , the leading asymptotic behavior of G_n is

$$G_n \sim \frac{1 + (-1)^n}{2} \frac{(-2)a_0}{\pi^{1/2}} n^{-3/2} z_*^{n+2} \quad (n \rightarrow \infty), \quad (\text{A.5})$$

which is associated with the $k = 0$ term.

The leading n dependence can also be deduced from the integral perspective. At large n , the leading contributions of (A.3) are localized near the largest eigenvalues $|z| \approx z_*$ which is shown in Fig. 9. They are not precisely at $z^2 = z_*^2$ because the eigenvalue density vanishes at the largest eigenvalue. We can determine the approximate location by $\frac{d}{dz}(z^n(z^2 - z_*^2)^{1/2}) = 0$, which gives the positions $z = \pm z_*(1 + 1/n)^{-1/2}$ and the maximum integrand $\text{Max}[z^n(z^2 - z_*^2)^{1/2}] \approx (en)^{-1/2} z_*^{n+1}$. We can also estimate the width of the localized region by $\frac{d^2}{dz^2}(z^n(z^2 - z_*^2)^{1/2}) = 0$, which gives $z \approx \pm(1 - (1 + 2^{1/2})/(2n))z_*$. The leading n dependence of G_n can be deduced from a product of the height and width $(n^{-1/2} z_*^{n+1})(n^{-1} z_*) = n^{-3/2} z_*^{n+2}$, which is consistent with the asymptotic behavior in (A.5).

For multi-length Green's functions, it is natural to expect that the leading contributions in the large length limit also localize around the largest eigenvalues $|z| = z_*$, which correspond to the edges of the supports of the eigenvalue distributions. Therefore, the large length limit of the multi-length Green's functions is dominated by a factorized term, such as the two-length case in (3.37).

References

- [1] W. Li, "Null bootstrap for non-Hermitian Hamiltonians," Phys. Rev. D **106**, no.12, 125021 (2022) doi:10.1103/PhysRevD.106.125021 [arXiv:2202.04334 [hep-th]].
- [2] C. M. Bender, C. Karapoulitidis and S. P. Klevansky, "Underdetermined Dyson-Schwinger Equations," Phys. Rev. Lett. **130**, no.10, 101602 (2023) doi:10.1103/PhysRevLett.130.101602 [arXiv:2211.13026 [math-ph]].
- [3] C. M. Bender, C. Karapoulitidis and S. P. Klevansky, "Dyson-Schwinger equations in zero dimensions and polynomial approximations," Phys. Rev. D **108**, no.5, 056002 (2023) doi:10.1103/PhysRevD.108.056002 [arXiv:2307.01008 [math-ph]].
- [4] W. Li, "Taming Dyson-Schwinger Equations with Null States," Phys. Rev. Lett. **131**, no.3, 031603 (2023) doi:10.1103/PhysRevLett.131.031603 [arXiv:2303.10978 [hep-th]].
- [5] W. Li, "Principle of minimal singularity for Green's functions," Phys. Rev. D **109**, no.4, 045012 (2024) doi:10.1103/PhysRevD.109.045012 [arXiv:2309.02201 [hep-th]].
- [6] W. Li, "The ϕ^n trajectory bootstrap," [arXiv:2402.05778 [hep-th]].
- [7] F. J. Dyson, "The S matrix in quantum electrodynamics," Phys. Rev. **75**, 1736-1755 (1949) doi:10.1103/PhysRev.75.1736
- [8] J. S. Schwinger, "On the Green's functions of quantized fields. 1.," Proc. Nat. Acad. Sci. **37**, 452-455 (1951) doi:10.1073/pnas.37.7.452
- [9] J. S. Schwinger, "On the Green's functions of quantized fields. 2.," Proc. Nat. Acad. Sci. **37**, 455-459 (1951) doi:10.1073/pnas.37.7.455
- [10] H. W. Lin, "Bootstraps to strings: solving random matrix models with positivity," JHEP **06**, 090 (2020) doi:10.1007/JHEP06(2020)090 [arXiv:2002.08387 [hep-th]].
- [11] R. Rattazzi, V. S. Rychkov, E. Tonni and A. Vichi, "Bounding scalar operator dimensions in 4D CFT," JHEP **12**, 031 (2008) doi:10.1088/1126-6708/2008/12/031 [arXiv:0807.0004 [hep-th]].

- [12] P. D. Anderson and M. Kruczenski, “Loop Equations and bootstrap methods in the lattice,” Nucl. Phys. B **921**, 702-726 (2017) doi:10.1016/j.nuclphysb.2017.06.009 [arXiv:1612.08140 [hep-th]].
- [13] A. Jevicki, O. Karim, J. P. Rodrigues and H. Levine, “Loop Space Hamiltonians and Numerical Methods for Large N Gauge Theories,” Nucl. Phys. B **213**, 169-188 (1983) doi:10.1016/0550-3213(83)90180-3
- [14] A. Jevicki, O. Karim, J. P. Rodrigues and H. Levine, “Loop Space Hamiltonians and Numerical Methods for Large N Gauge Theories. 2.,” Nucl. Phys. B **230**, 299-316 (1984) doi:10.1016/0550-3213(84)90215-3
- [15] R. d. Koch, A. Jevicki, X. Liu, K. Mathaba and J. P. Rodrigues, “Large N optimization for multi-matrix systems,” JHEP **01**, 168 (2022) doi:10.1007/JHEP01(2022)168 [arXiv:2108.08803 [hep-th]].
- [16] K. Mathaba, M. Mulokwe and J. P. Rodrigues, “Large N master field optimization: the quantum mechanics of two Yang-Mills coupled matrices,” JHEP **02**, 054 (2024) doi:10.1007/JHEP02(2024)054 [arXiv:2306.00935 [hep-th]].
- [17] H. Hessam, M. Khalkhali and N. Pagliaroli, “Bootstrapping Dirac ensembles,” J. Phys. A **55**, no.33, 335204 (2022) [arXiv:2107.10333 [hep-th]].
- [18] M. Cho, B. Gabai, Y. H. Lin, V. A. Rodriguez, J. Sandor and X. Yin, “Bootstrapping the Ising Model on the Lattice,” [arXiv:2206.12538 [hep-th]].
- [19] X. Han, S. A. Hartnoll and J. Kruthoff, “Bootstrapping Matrix Quantum Mechanics,” Phys. Rev. Lett. **125**, no.4, 041601 (2020) doi:10.1103/PhysRevLett.125.041601 [arXiv:2004.10212 [hep-th]].
- [20] D. Berenstein and G. Hulsey, “Bootstrapping Simple QM Systems,” [arXiv:2108.08757 [hep-th]].
- [21] J. Bhattacharya, D. Das, S. K. Das, A. K. Jha and M. Kundu, “Numerical bootstrap in quantum mechanics,” Phys. Lett. B **823** (2021), 136785 [arXiv:2108.11416 [hep-th]].
- [22] Y. Aikawa, T. Morita and K. Yoshimura, “Application of bootstrap to a θ term,” Phys. Rev. D **105** (2022) no.8, 085017 [arXiv:2109.02701 [hep-th]].
- [23] D. Berenstein and G. Hulsey, “Bootstrapping more QM systems,” J. Phys. A **55** (2022) no.27, 275304 [arXiv:2109.06251 [hep-th]].
- [24] S. Tchoumakov and S. Florens, “Bootstrapping Bloch bands,” J. Phys. A **55** (2022) no.1, 015203 [arXiv:2109.06600 [cond-mat.mes-hall]].
- [25] Y. Aikawa, T. Morita and K. Yoshimura, “Bootstrap method in harmonic oscillator,” Phys. Lett. B **833** (2022), 137305 [arXiv:2109.08033 [hep-th]].
- [26] B. n. Du, M. x. Huang and P. x. Zeng, “Bootstrapping Calabi–Yau quantum mechanics,” Commun. Theor. Phys. **74** (2022) no.9, 095801 [arXiv:2111.08442 [hep-th]].
- [27] S. Lawrence, “Bootstrapping Lattice Vacua,” [arXiv:2111.13007 [hep-lat]].
- [28] D. Bai, “Bootstrapping the deuteron,” [arXiv:2201.00551 [nucl-th]].
- [29] Y. Nakayama, “Bootstrapping microcanonical ensemble in classical system,” Mod. Phys. Lett. A **37** (2022) no.09, 2250054 [arXiv:2201.04316 [hep-th]].
- [30] S. Khan, Y. Agarwal, D. Tripathy and S. Jain, “Bootstrapping PT symmetric quantum mechanics,” Phys. Lett. B **834** (2022), 137445 [arXiv:2202.05351 [quant-ph]].

- [31] D. Berenstein and G. Hulsey, “Anomalous bootstrap on the half-line,” *Phys. Rev. D* **106**, no.4, 045029 (2022) [arXiv:2206.01765 [hep-th]].
- [32] T. Morita, “Universal bounds on quantum mechanics through energy conservation and the bootstrap method,” *PTEP* **2023** (2023) no.2, 023A01 [arXiv:2208.09370 [hep-th]].
- [33] M. J. Blacker, A. Bhattacharyya and A. Banerjee, “Bootstrapping the Kronig-Penney model,” *Phys. Rev. D* **106** (2022) no.11, 11 [arXiv:2209.09919 [quant-ph]].
- [34] D. Berenstein and G. Hulsey, “Semidefinite programming algorithm for the quantum mechanical bootstrap,” *Phys. Rev. E* **107** (2023) no.5, L053301 [arXiv:2209.14332 [hep-th]].
- [35] S. Lawrence, “Semidefinite programs at finite fermion density,” *Phys. Rev. D* **107** (2023) no.9, 094511 [arXiv:2211.08874 [hep-lat]].
- [36] H. W. Lin, “Bootstrap bounds on D0-brane quantum mechanics,” *JHEP* **06** (2023), 038 [arXiv:2302.04416 [hep-th]].
- [37] Y. Guo and W. Li, “Solving anharmonic oscillator with null states: Hamiltonian bootstrap and Dyson-Schwinger equations,” *Phys. Rev. D* **108**, no.12, 125002 (2023) doi:10.1103/PhysRevD.108.125002 [arXiv:2305.15992 [hep-th]].
- [38] D. Berenstein and G. Hulsey, “One-dimensional reflection in the quantum mechanical bootstrap,” *Phys. Rev. D* **109**, no.2, 025013 (2024) doi:10.1103/PhysRevD.109.025013 [arXiv:2307.11724 [hep-th]].
- [39] W. Fan and H. Zhang, “Non-perturbative instanton effects in the quartic and the sextic double-well potential by the numerical bootstrap approach,” [arXiv:2308.11516 [hep-th]].
- [40] R. R. John and K. P. R., “Anharmonic oscillators and the null bootstrap,” [arXiv:2309.06381 [quant-ph]].
- [41] W. Fan and H. Zhang, “A non-perturbative formula unifying double-wells and anharmonic oscillators under the numerical bootstrap approach,” [arXiv:2309.09269 [quant-ph]].
- [42] X. Han, “Quantum Many-body Bootstrap,” [arXiv:2006.06002[cond-mat]].
- [43] C. O. Nancarrow and Y. Xin, “Bootstrapping the gap in quantum spin systems,” *JHEP* **08**, 052 (2023) doi:10.1007/JHEP08(2023)052 [arXiv:2211.03819 [hep-th]].
- [44] I. Kull, N. Schuch, B. Dive and M. Navascués, “Lower Bounds on Ground-State Energies of Local Hamiltonians through the Renormalization Group,” *Phys. Rev. X* **14**, no.2, 021008 (2024) doi:10.1103/PhysRevX.14.021008 [arXiv:2212.03014 [quant-ph]].
- [45] D. Berenstein, G. Hulsey and P. N. T. Lloyd, “Numerical exploration of the bootstrap in spin chain models,” [arXiv:2406.17844 [hep-th]].
- [46] V. Kazakov and Z. Zheng, “Analytic and numerical bootstrap for one-matrix model and “unsolvable” two-matrix model,” *JHEP* **06**, 030 (2022) doi:10.1007/JHEP06(2022)030 [arXiv:2108.04830 [hep-th]].
- [47] V. Kazakov and Z. Zheng, “Bootstrap for lattice Yang-Mills theory,” *Phys. Rev. D* **107**, no.5, L051501 (2023) doi:10.1103/PhysRevD.107.L051501 [arXiv:2203.11360 [hep-th]].
- [48] V. Kazakov and Z. Zheng, “Bootstrap for Finite N Lattice Yang-Mills Theory,” [arXiv:2404.16925 [hep-th]].
- [49] Z. Li and S. Zhou, “Bootstrapping the Abelian Lattice Gauge Theories,” [arXiv:2404.17071 [hep-th]].

- [50] V. A. Kazakov, “Solvable matrix models,” [arXiv:hep-th/0003064 [hep-th]].
- [51] A. L. Fitzpatrick, J. Kaplan, D. Poland and D. Simmons-Duffin, “The Analytic Bootstrap and AdS Superhorizon Locality,” JHEP **12**, 004 (2013) doi:10.1007/JHEP12(2013)004 [arXiv:1212.3616 [hep-th]].
- [52] Z. Komargodski and A. Zhiboedov, “Convexity and Liberation at Large Spin,” JHEP **11**, 140 (2013) doi:10.1007/JHEP11(2013)140 [arXiv:1212.4103 [hep-th]].
- [53] H. A. Kramers and G. H. Wannier, “Statistics of the two-dimensional ferromagnet. Part 1.,” Phys. Rev. **60**, 252-262 (1941) doi:10.1103/PhysRev.60.252
- [54] H. A. Kramers and G. H. Wannier, “Statistics of the Two-Dimensional Ferromagnet. Part II,” Phys. Rev. **60**, 263-276 (1941) doi:10.1103/PhysRev.60.263
- [55] L. Onsager, “Crystal statistics. 1. A Two-dimensional model with an order disorder transition,” Phys. Rev. **65**, 117-149 (1944) doi:10.1103/PhysRev.65.117
- [56] B. Eynard, T. Kimura and S. Ribault, “Random matrices,” [arXiv:1510.04430 [math-ph]].
- [57] E. Brezin, C. Itzykson, G. Parisi and J. B. Zuber, “Planar Diagrams,” Commun. Math. Phys. **59**, 35 (1978) doi:10.1007/BF01614153
- [58] R. G. Jha, “Introduction to Monte Carlo for matrix models,” SciPost Phys. Lect. Notes **46**, 1 (2022) doi:10.21468/SciPostPhysLectNotes.46 [arXiv:2111.02410 [hep-th]].
- [59] M. Staudacher, “Combinatorial solution of the two matrix model,” Phys. Lett. B **305**, 332-338 (1993) doi:10.1016/0370-2693(93)91063-S [arXiv:hep-th/9301038 [hep-th]].
- [60] L. F. Alday and J. M. Maldacena, “Comments on operators with large spin,” JHEP **11**, 019 (2007) doi:10.1088/1126-6708/2007/11/019 [arXiv:0708.0672 [hep-th]].
- [61] L. F. Alday, “Large Spin Perturbation Theory for Conformal Field Theories,” Phys. Rev. Lett. **119**, no.11, 111601 (2017) doi:10.1103/PhysRevLett.119.111601 [arXiv:1611.01500 [hep-th]].
- [62] L. F. Alday, “Solving CFTs with Weakly Broken Higher Spin Symmetry,” JHEP **10**, 161 (2017) doi:10.1007/JHEP10(2017)161 [arXiv:1612.00696 [hep-th]].
- [63] D. Simmons-Duffin, “The Lightcone Bootstrap and the Spectrum of the 3d Ising CFT,” JHEP **03**, 086 (2017) doi:10.1007/JHEP03(2017)086 [arXiv:1612.08471 [hep-th]].
- [64] S. Caron-Huot, “Analyticity in Spin in Conformal Theories,” JHEP **1709**, 078 (2017) doi:10.1007/JHEP09(2017)078 [arXiv:1703.00278 [hep-th]].
- [65] W. Li, “Easy bootstrap for the 3D Ising model: a hybrid approach of the lightcone bootstrap and error minimization methods,” JHEP **07**, 047 (2024) doi:10.1007/JHEP07(2024)047 [arXiv:2312.07866 [hep-th]].
- [66] J. Hoppe, “Quantum Theory Of A Massless Relativistic Surface And A Two Dimensional Bound State Problem, Ph.D. Thesis, Massachusetts Institute of Technology (1982).”
- [67] V. A. Kazakov, I. K. Kostov and N. A. Nekrasov, “D particles, matrix integrals and KP hierarchy,” Nucl. Phys. B **557**, 413-442 (1999) doi:10.1016/S0550-3213(99)00393-4 [arXiv:hep-th/9810035 [hep-th]].
- [68] D. Poland, S. Rychkov and A. Vichi, “The Conformal Bootstrap: Theory, Numerical Techniques, and Applications,” Rev. Mod. Phys. **91**, 015002 (2019) doi:10.1103/RevModPhys.91.015002 [arXiv:1805.04405 [hep-th]].

- [69] T. Hartman, D. Mazac, D. Simmons-Duffin and A. Zhiboedov, “Snowmass White Paper: The Analytic Conformal Bootstrap,” [arXiv:2202.11012 [hep-th]].
- [70] S. Rychkov and N. Su, “New Developments in the Numerical Conformal Bootstrap,” [arXiv:2311.15844 [hep-th]].
- [71] N. Ishibashi, H. Kawai, Y. Kitazawa and A. Tsuchiya, “A Large N reduced model as superstring,” Nucl. Phys. B **498**, 467-491 (1997) doi:10.1016/S0550-3213(97)00290-3 [arXiv:hep-th/9612115 [hep-th]].
- [72] T. Banks, W. Fischler, S. H. Shenker and L. Susskind, “M theory as a matrix model: A Conjecture,” Phys. Rev. D **55**, 5112-5128 (1997) doi:10.1103/PhysRevD.55.5112 [arXiv:hep-th/9610043 [hep-th]].
- [73] D. E. Berenstein, J. M. Maldacena and H. S. Nastase, “Strings in flat space and pp waves from N=4 superYang-Mills,” JHEP **04**, 013 (2002) doi:10.1088/1126-6708/2002/04/013 [arXiv:hep-th/0202021 [hep-th]].